# Analytic description of the above-threshold detachment in the adiabatic limit

A. V. Flegel,[1] N. L. Manakov,[1] A. V. Sviridov,[1,2] M. V. Frolov,[1,2] Lei Geng,[3] and Liang-You Peng[3,4,5]

[1]*Department of Physics, Voronezh State University, Voronezh 394018, Russia*

[2]*Department of Radiophysics, University of Nizhny Novgorod, Nizhny Novgorod 603950, Russia*

[3]*State Key Laboratory for Mesoscopic Physics and Frontiers Science Center for Nano-optoelectronics, School of Physics, Peking University, 100871 Beijing, China*

[4]*Collaborative Innovation Center of Extreme Optics, Shanxi University, 030006 Taiyuan, China*

[5]*Beijing Academy of Quantum Information Sciences , Beijing 100193, China*

(Received 11 September 2020; revised 27 October 2020; accepted 10 November 2020; published 24 December 2020)

Strong-field above-threshold detachment (ATD) is analyzed in the low-frequency (or adiabatic) limit. The explicit form of ATD amplitude is obtained within a developed low-frequency approximation. We show that in the low-frequency limit, the atomic structure effects are introduced in the ATD amplitude through the $T$ matrix, which in the limiting case coincides with the amplitude of elastic electron scattering. The rescattering part of ATD amplitude is evaluated in terms of the closed *real* classical electron trajectories. We further discuss the behavior of ATD amplitude near the caustic rescattering energies (classical energies for which two trajectories merge into a single one) of photoelectrons. Comparison of developed analytic theory with the numerical solution of time-dependent Schrödinger equation is presented for linearly polarized and time-delayed bicircular fields. Based on the analytical description, we predict an enhancement of ATD yield for time-delayed bicircular fields, which is similar to previous findings for the high harmonic yield [M.V. Frolov *et al.*, Phys. Rev. Lett. **120**, 263203 (2018)].

DOI: 10.1103/PhysRevA.102.063119

## I. INTRODUCTION

Above-threshold ionization/detachment (ATI/ATD) is a fundamental process in an intense laser field, which has attracted a steady interest for more than 50 years. For a long laser pulse, ATI/ATD is understood as absorption of more laser photons than that needed for ionization with subsequent production of photoelectrons with equidistant energies separated by one photon energy [1–3]. For a short (few-cycle) pulse, this photoelectron energy comb is smeared out [4] and more specific short-pulse-related effects are shown up in ATI/ATD spectra [5]. Although physical channels of nonlinear ionization were established more than 50 years ago [6–8], up to now new theoretical models and approaches have been suggested to describe new effects in the spectra of ATI/ATD. The main cornerstone of any new approaches or models is to take into account on equal footing both the nonperturbative electron-laser interaction and atomic dynamics (including effects of the long-range Coulomb field), which may be modified by a laser field. The quality of suggested theoretical models and approaches is mostly tested by comparison with the numerical solution of time-dependent Schrödinger equation (TDSE), which takes into account laser-atom interaction and atomic structure effects, possibly better, than any analytical model or other approaches. Although numerical TDSE solution provides *ab inito* results, its ability is quite restricted by the intensity, wavelength, and wave form of a laser pulse and it presents a time-consuming task for an intense tailored laser pulse having carrier frequencies in the midinfrared (mid-IR) range ($2\ \mu\text{m} < \lambda < 50\ \mu\text{m}$) and intensities $\gtrsim 10^{14}$ W/cm$^2$. We note, that numerical TDSE results cannot provide a fundamental insight into physical problem, since they are obtained for particular values of parameters. Moreover, some applications in physics require a robust analytical expression for probability of a fundamental process in an intense laser field with accuracy comparable with time-consuming numerical *ab initio* results. Such analytical expressions significantly speed up the efficiency of existing heavy codes in plasma physics, e.g., particle-in-cell codes. The robust analytical expressions can be obtained within analytical methods, whose implementation in physical problems is extremely important. The nonlinear interaction of an intense mid-IR field with an atomic or molecular target is a perfect example, for which analytical methods can be applied. Indeed, parameters of the intense mid-IR laser field are perfect for the quasiclassical treatment of nonlinear ionization, which is ensured by inequalities: $\hbar\omega \ll I_p$ and $S \gg \hbar$, where $\omega$, $I_p$, and $S$ represent the typical carrier frequency, ionization potential, and classical action of the photoelectron in the laser field, respectively.

Most of theoretical approaches are based on the $S$-matrix formalism [3,5,9,10]. Expansion of $S$-matrix element in a formal series in an atomic potential leads to a Born-like form for the ionization amplitude, so that each term of this expansion is determined by the transition between a field-free bound state and the continuum plane-wave Volkov state. Further simplification is achieved by estimating spatial and temporal integrals for each constituent of a total transition amplitude

 ©2020 American Physical Society

within the saddle-point method [11]. The corresponding equations for saddle points present specific conditions for adiabatic transitions [12], i.e., each quantum transition is realized at the instants of time (in general, complex) for which energies of "initial" and "final" states are the same. Due to the Born expansion of transition amplitudes (i.e., matrix elements are presented in terms of the Green's function and wave function of a free electron in a laser field), these conditions involve the energy of a free electron in a laser field. The corresponding instants of adiabatic transitions may be also interpreted as starting and ending times of electron moving along trajectories, which formally obey Newton equations, and each constituent of the transition amplitude can be presented as a coherent sum of partial amplitudes associated with the corresponding (closed or unclosed) classical trajectories [3,9,13].

The dynamics of an atomic system in an intense low-frequency field is also considered successfully in the adiabatic approximation. The general idea of this approximation consists in the utilization of smallness of carrier frequency for quasistatic expansion of the laser-distorted wave function [14–18]. In these publications, the low energy part of ATI/ATD spectra or either total ionization/detachment rate are considered for an atomic system subjected to a periodic linearly polarized field. In Refs. [19–21], one can find the further development of the adiabatic theory consisting of the calculation of the rescattering part of the wave function on the adiabatic basis. Within the adiabatic approach, both low-energy and high-energy (or rescattering) parts of photoelectron spectra have been calculated. Adiabatic approximation also is used in the model calculations [22–24]. In the latter case, the adiabatic solution of model-dependent equations is suggested together with the evaluation of corresponding matrix elements based on the smallness of the underbarrier time with respect to the period of a laser field (see also Ref. [25]). It should be noted that results of Refs. [22–24] are obtained within the analytical time-dependent effective range (TDER) model [26,27], which supports only a finite number of scattering phases, so that the extension of model TDER results to the real systems has been made heuristically.

In this work, we present an alternative to the existing theoretical approaches. Our approach is based on the analysis of integral equation for the quasistationary quasienergy state (QQES) in a periodic laser field for an arbitrary short-range potential [28–31]. We show that the integral equation for QQES can be transformed to a form similar to that for the TDER model [22,24], however, in contrast to the TDER model, this equation involves explicitly the Fourier-transform of a short-range potential [see Eq. (10)]. This result allows one to develop a low-frequency approximation for the detachment amplitude. Based on the developed approach, we show that the rescattering part of the ATD amplitude is expressed in terms of the $T$ matrix for collision problems [32], which determines the amplitude of the elastic electron scattering. This result provides fundamental corrections to the dependence of ATD amplitude on the atomic potential, e.g., the factorization of ATI/ATD amplitude in terms of the electron scattering cross section [19,21,22,24,33–39] and its validation for short pulses [23]. It should be noted, that in Ref. [37] the ATD amplitude also was expressed in terms of $T$ matrix, however, the mathematical rigor of the methods used in Ref. [37] is questionable and additional justification is needed (see Ref. [22] in Ref. [40]). We also extend our recently developed approach for high harmonic generation [41,42] to the case of ATD and express the detachment amplitude in terms of partial amplitudes associated with closed real electron trajectories. These closed real trajectories can be parametrized in terms of corresponding real starting and finishing times, which are key ingredients of our theory.

The paper is organized as follows: in Sec. II we discuss the general theoretical background for ATD; in Sec. III we analyze ATD amplitude in the low-frequency approximation; in Sec. IV we present a comparison of our analytical approach with the numerical solution of TDSE and discuss the enhancement in the ATD yield for bicircular field; in Sec. V we summarize our results. All necessary mathematical details are given in Appendixes A–C, as well as details of the numerical solution of TDSE presented in Appendix D. Atomic units (a.u.) are used throughout this paper unless specified otherwise.

## II. THEORETICAL BACKGROUND

We shall analyze the strong-field detachment of a weakly bound electron, which interacts with a periodic laser field. The electron-laser interaction $V(\boldsymbol{r},t)$ is considered in the dipole approximation (the length gauge is used):

$$V(\boldsymbol{r},t)=\boldsymbol{r}\cdot\boldsymbol{F}(t),\quad \boldsymbol{F}(t+\mathcal{T})=\boldsymbol{F}(t),$$

where $\boldsymbol{F}(t)$ is the electric component of a periodic laser field with period $\mathcal{T}$. In order to describe self-consistently the detachment process in a strong periodic laser field, we use the QQES approach [28,29,31]. In the frame of the QQES approach, the exact wave function, $\Psi_\epsilon(\boldsymbol{r},t)$, has the form

$$\Psi_\epsilon(\boldsymbol{r},t)=e^{-i\epsilon t}\Phi_\epsilon(\boldsymbol{r},t),\quad \Phi_\epsilon(\boldsymbol{r},t)=\Phi_\epsilon(\boldsymbol{r},t+\mathcal{T}),$$

whose periodic part $\Phi_\epsilon(\boldsymbol{r},t)$ obeys the "stationary" Schrödinger equation:

$$\left[-\frac{\nabla^2}{2}+U(r)+V(\boldsymbol{r},t)-i\frac{\partial}{\partial t}\right]\Phi_\epsilon(\boldsymbol{r},t)=\epsilon\Phi_\epsilon(\boldsymbol{r},t),\quad (1)$$

where $U(r)$ is a short-range potential. Equation (1) is supplemented by the spherical outgoing wave boundary condition at large distances, which ensures the complexity of quasienergy $\epsilon$ [28–31]. The eigenvalue problem (1) can be also formulated in terms of the *homogeneous* integral equation:

$$\Phi_\epsilon(\boldsymbol{r},t)=\int_{-\infty}^{t}dt'\int d\boldsymbol{r}'e^{i\epsilon(t-t')}G(\boldsymbol{r},t;\boldsymbol{r}',t')\times U(r')\Phi_\epsilon(\boldsymbol{r}',t'),\quad (2)$$

where $G(\boldsymbol{r},t;\boldsymbol{r}',t')$ is the retarded nonstationary Green's function of the free electron in a laser field (see, e.g., Appendix B in Ref. [30]).[1] As can be shown, at large distances from Eq. (2) follows an expansion of QQES wave function in terms

[1]One should notice that in the QQES approach, all integrals are considered in the sense of analytic continuation in $\epsilon$ (see discussions in Ref. [30]).

of outgoing spherical waves (see Ref. [17] and Appendix A for details):

$$\Phi_\epsilon(\boldsymbol{r},t)\big|_{r\to\infty} \propto \sum_n \mathcal{A}(\boldsymbol{p}_n)\frac{e^{ip_n|\boldsymbol{R}(\boldsymbol{r},t)|-in\omega_\tau t}}{|\boldsymbol{R}(\boldsymbol{r},t)|},$$
$$\boldsymbol{R}(\boldsymbol{r},t)=\boldsymbol{r}-\int^t \boldsymbol{A}(\xi)d\xi,$$
$$\boldsymbol{p}_n^2/2=\epsilon-u_p+n\omega_\tau,\quad \omega_\tau=2\pi/\mathcal{T},$$
$$u_p=\frac{1}{2\mathcal{T}}\int_{-\mathcal{T}/2}^{\mathcal{T}/2}\boldsymbol{A}^2(\xi)d\xi,\quad \boldsymbol{F}(t)=-\frac{\partial \boldsymbol{A}(t)}{\partial t}, \tag{3}$$

where $\boldsymbol{A}(t)$ is the vector potential of a laser field, $\mathcal{A}(\boldsymbol{p}_n)$ is the detachment amplitude, and $\boldsymbol{p}_n$ is the momentum of the detached electron after the absorption of $n$ photons with energy $\omega_\tau$. The detachment amplitude, $\mathcal{A}(\boldsymbol{p}_n)$, can be presented in the form:

$$\mathcal{A}(\boldsymbol{p}_n)=-\frac{1}{2\pi\mathcal{T}}\int_{-\mathcal{T}/2}^{\mathcal{T}/2}dt\,e^{in\omega_\tau t}\times\int d\boldsymbol{r}\,\chi^*_{\boldsymbol{p}_n}(\boldsymbol{r},t)U(r)\Phi_\epsilon(\boldsymbol{r},t), \tag{4}$$

where

$$\chi_{\boldsymbol{p}}(\boldsymbol{r},t)=e^{i\{\boldsymbol{P}(t)\cdot\boldsymbol{r}-\int^t[\boldsymbol{p}\cdot\boldsymbol{A}(\tau)+\boldsymbol{A}^2(\tau)/2]d\tau-u_p t\}},$$
$$\boldsymbol{P}(t)=\boldsymbol{p}+\boldsymbol{A}(t). \tag{5}$$

For our further analysis, we present the QQES wave function in the momentum representation:

$$\Phi_\epsilon(\boldsymbol{r},t)=\int e^{i\boldsymbol{K}(t)\cdot\boldsymbol{r}}\varphi_\epsilon(\boldsymbol{k},t)d\boldsymbol{k},\quad \boldsymbol{K}(t)=\boldsymbol{k}+\boldsymbol{A}(t). \tag{6}$$

Substituting expansion (6) into Eq. (2) and taking into account the expansion of the Green's function

$$G(\boldsymbol{r},t;\boldsymbol{r}',t')=-i(2\pi)^{-3}\int\chi^*_{\boldsymbol{q}}(\boldsymbol{r}',t')\times\chi_{\boldsymbol{q}}(\boldsymbol{r},t)e^{-i(\frac{q^2}{2}+u_p)(t-t')}d\boldsymbol{q}, \tag{7}$$

we obtain the equation for $\varphi_\epsilon(\boldsymbol{k},t)$:

$$\varphi_\epsilon(\boldsymbol{k},t)=-i\int_{-\infty}^t dt'\,e^{iS_\epsilon(\boldsymbol{k};t,t')}\times\int d\boldsymbol{k}'u(\boldsymbol{k}-\boldsymbol{k}')\varphi_\epsilon(\boldsymbol{k}',t'), \tag{8}$$

where

$$S_\epsilon(\boldsymbol{k};t,t')=\epsilon(t-t')-\frac{1}{2}\int_{t'}^t\boldsymbol{K}^2(\tau)d\tau, \tag{9a}$$
$$u(\boldsymbol{k})=u(|\boldsymbol{k}|)=\frac{1}{(2\pi)^3}\int e^{-i\boldsymbol{k}\cdot\boldsymbol{r}}U(r)d\boldsymbol{r}. \tag{9b}$$

Multiplying both sides of Eq. (8) with $u(\boldsymbol{p}-\boldsymbol{k})$ and integrating in $\boldsymbol{k}$, we obtain the homogeneous integral equation

$$f_\epsilon(\boldsymbol{p},t)=-i\int_{-\infty}^t dt'\int d\boldsymbol{k}e^{iS_\epsilon(\boldsymbol{k};t,t')}u(\boldsymbol{p}-\boldsymbol{k})f_\epsilon(\boldsymbol{k},t'), \tag{10}$$

where

$$f_\epsilon(\boldsymbol{p},t)=\int u(\boldsymbol{p}-\boldsymbol{k})\varphi_\epsilon(\boldsymbol{k},t)d\boldsymbol{k}. \tag{11}$$

In terms of the function $f_\epsilon(\boldsymbol{p},t)$, the ATD amplitude (4) takes the form

$$\mathcal{A}(\boldsymbol{p}_n)=-\frac{4\pi^2}{\mathcal{T}}\int_{-\mathcal{T}/2}^{\mathcal{T}/2}e^{iS_{p_n}(t)}f_\epsilon(\boldsymbol{p}_n,t)dt,$$
$$S_{p_n}(t)=\int^t\frac{\boldsymbol{P}_n^2(\tau)}{2}d\tau-\epsilon t,\quad \boldsymbol{P}_n(t)=\boldsymbol{p}_n+\boldsymbol{A}(t). \tag{12}$$

We notice that Eqs. (10) and (12) are similar to those obtained in the framework of the TDER theory [c.f., Eq. (29) from Ref. [43] with Eq. (10) and Eq. (26) from Ref. [24] with Eq. (12)], however, in contrast to the TDER theory, the solution of Eq. (10) is sensitive to the shape of an atomic potential $U(r)$.

## III. LOW-FREQUENCY APPROXIMATION

In this section, we analyze the integral equation (10) and the ATD amplitude (12) in the low-frequency (or adiabatic) limit, whose validity is ensured by inequalities: $F^2/\omega^3 \gg 1$ and $I_p/\omega \gg 1$, where $F$ and $\omega$ give the order of magnitude for strength and carrier frequency of a strong low-frequency laser field and $I_p$ is the detachment threshold. These inequalities ensure the application of quasiclassical approximation, whose mathematical background is based on the evaluation of ionization amplitude by the saddle-point method [5–9,13].

### A. Low-frequency approximation for $f_\epsilon(\mathbf{p},t)$

In the low-frequency limit, we separate $f_\epsilon(\boldsymbol{p},t)$ into two parts:

$$f_\epsilon(\boldsymbol{p},t)=f_\epsilon^{(s)}(\boldsymbol{p},t)+f_\epsilon^{(r)}(\boldsymbol{p},t), \tag{13}$$

where $f_\epsilon^{(s)}(\boldsymbol{p},t)$ is a slowly varying function and $f_\epsilon^{(r)}(\boldsymbol{p},t)$ is a rapidly oscillating function in time:

$$\frac{1}{\mathcal{T}}\int_{-\mathcal{T}/2}^{\mathcal{T}/2}f_\epsilon^{(s)}(\boldsymbol{p},t)f_\epsilon^{(r)}(\boldsymbol{p},t)dt\ll 1.$$

We substitute expansion (13) into Eq. (10) and arrive at

$$f_\epsilon^{(s)}(\boldsymbol{p},t)+f_\epsilon^{(r)}(\boldsymbol{p},t)=-i\int_{-\infty}^t dt'\int d\boldsymbol{k}\,e^{iS_\epsilon(\boldsymbol{k};t,t')}u(\boldsymbol{p}-\boldsymbol{k})f_\epsilon^{(s)}(\boldsymbol{k},t')-i\int_{-\infty}^t dt'\int d\boldsymbol{k}\,e^{iS_\epsilon(\boldsymbol{k};t,t')}u(\boldsymbol{p}-\boldsymbol{k})f_\epsilon^{(r)}(\boldsymbol{k},t'). \tag{14}$$

The temporal integral in the second line of Eq. (14) can be analytically estimated since fast and slow parts of integrand are explicitly separated. There are two contributions in this temporal integral (see, e.g., Ref. [11]): (i) contribution from the vicinity of the upper limit; (ii) contribution from saddle points [see Eq. (17)]. The first integral in Eq. (14) takes the

form

$$-i\int_{-\infty}^{t}dt'\int d\boldsymbol{k}\,e^{iS_\epsilon(\boldsymbol{k};t,t')}u(\boldsymbol{p}-\boldsymbol{k})f_\epsilon^{(s)}(\boldsymbol{k},t') \approx \int\frac{u(\boldsymbol{p}-\boldsymbol{k})f_\epsilon^{(s)}(\boldsymbol{k},t)}{\epsilon-\boldsymbol{K}^2(t)/2+i0}d\boldsymbol{k}+c_\epsilon(\boldsymbol{p},t), \tag{15}$$

where $c_\epsilon(\boldsymbol{p},t)$ represents the saddle-point contribution,

$$c_\epsilon(\boldsymbol{p},t)=2\pi\sum_s\int\frac{e^{iS_\epsilon(\boldsymbol{k};t,t_s')}}{\sqrt{2\pi i\alpha_s}} \times u(\boldsymbol{p}-\boldsymbol{k})f_\epsilon^{(s)}(\boldsymbol{k},t_s')d\boldsymbol{k},$$
$$\alpha_s\equiv\alpha_s(\boldsymbol{k})=\frac{\partial^2}{\partial t'^2}S_\epsilon(\boldsymbol{k};t,t')\Big|_{t'=t_s'}=\boldsymbol{K}(t_s')\cdot\boldsymbol{F}(t_s'). \tag{16}$$

In Eq. (16), saddle points $t'_s\equiv t_s'(\boldsymbol{k})$ obey the equation

$$\boldsymbol{K}^2(t_s')=2\epsilon, \tag{17}$$

and a summation is taken for all appropriate saddle points.

The first term in Eq. (15) slowly varies in time, while the second one changes rapidly. Using Eq. (15), we separate from Eq. (14) equations for "slow" and "fast" parts of the function $f_\epsilon(\boldsymbol{p},t)$:

$$f_\epsilon^{(s)}(\boldsymbol{p},t)=\int\frac{u(\boldsymbol{p}-\boldsymbol{k})f_\epsilon^{(s)}(\boldsymbol{k},t)}{\epsilon-\boldsymbol{K}^2(t)/2+i0}d\boldsymbol{k}, \tag{18a}$$

$$f_\epsilon^{(r)}(\boldsymbol{p},t)=c_\epsilon(\boldsymbol{p},t)-i\int_{-\infty}^{t}dt''\int d\tilde{\boldsymbol{k}}\,e^{iS_\epsilon(\tilde{\boldsymbol{k}};t,t'')} \times u(\boldsymbol{p}-\tilde{\boldsymbol{k}})f_\epsilon^{(r)}(\tilde{\boldsymbol{k}},t''), \tag{18b}$$

where Eq. (18a) is for the slowly varying part, $f_\epsilon^{(s)}(\boldsymbol{p},t)$, and Eq. (18b) is for the rapidly varying part, $f_\epsilon^{(r)}(\boldsymbol{p},t)$ [in the integral term of Eq. (18b) we renamed $t'\to t''$ and $\boldsymbol{k}\to\tilde{\boldsymbol{k}}$ for further convenience].

The solution of Eq. (18a) can be expressed in terms of the field-free solution. Indeed, for the field-free case, $f_\epsilon(\boldsymbol{p},t)$ does not depend on the time and Eq. (10) is simplified:

$$f_{E_0}^{(0)}(\boldsymbol{p})=-i\int_{-\infty}^{t}dt'\int d\boldsymbol{k}\,e^{i(E_0-\boldsymbol{k}^2/2)(t-t')} \times u(\boldsymbol{p}-\boldsymbol{k})f_{E_0}^{(0)}(\boldsymbol{k}) =\int\frac{u(\boldsymbol{p}-\boldsymbol{k})f_{E_0}^{(0)}(\boldsymbol{k})}{E_0-k^2/2+i0}d\boldsymbol{k}, \tag{19}$$

where $E_0=-I_p$ is the energy of an initial bound state and $f_{E_0}^{(0)}(\boldsymbol{p})$ is given by the Fourier-transform of an initial state [see Eqs. (8), (9a), and (11) for field-free case]:

$$\varphi_0(\boldsymbol{k})=\frac{f_{E_0}^{(0)}(\boldsymbol{k})}{E_0-k^2/2+i0}. \tag{20}$$

Although the function $f_{E_0}^{(0)}(\boldsymbol{k})$ determines the field-free dynamics of initially bound electron in the whole momentum space, the contribution of this function to the amplitude of the strong field ionization is given by the vicinity of $k=\sqrt{2E_0}=i\kappa$ (see, e.g., Sec. 4 in Ref. [7]). It should be emphasized that $f_{E_0}^{(0)}(i\kappa\hat{\boldsymbol{k}})$ can be expressed in terms of the asymptotic coefficient $C_{\kappa l}$, which defines behavior of the initial state, $\psi_{E_0}(\boldsymbol{r})$, at large distances:

$$\psi_{E_0}(\boldsymbol{r})|_{\kappa r\gg1}\simeq C_{\kappa l}\frac{e^{-\kappa r}}{r}Y_{lm}(\hat{\boldsymbol{r}}), \tag{21}$$

where $Y_{lm}(\hat{\boldsymbol{r}})$ is the spherical harmonic, $l$ and $m$ are the angular momentum and magnetic quantum numbers of the bound electron in the initial state. Indeed, the asymptotic behavior (21) of the wave function $\psi_{E_0}(\boldsymbol{r})$ in coordinate space is determined by the pole $k=i\kappa$ in Eq. (20) for $\varphi_0(\boldsymbol{k})$ in the momentum space. Thus, evaluating the Fourier transform of Eq. (21) and comparing with Eq. (20), we obtain [cf. Eq. (50) in [7]]:

$$f_{E_0}^{(0)}(i\kappa\hat{\boldsymbol{k}})=-\frac{1}{4\pi^2}C_{\kappa l}Y_{lm}(\hat{\boldsymbol{k}}). \tag{22}$$

By taking into account Eq. (19) and equality $\boldsymbol{P}(t)-\boldsymbol{K}(t)=\boldsymbol{p}-\boldsymbol{k}$, where $\boldsymbol{P}(t)=\boldsymbol{p}+\boldsymbol{A}(t)$, it can be explicitly checked that

$$f_\epsilon^{(s)}(\boldsymbol{p},t)=f_{E_0}^{(0)}(\boldsymbol{P}(t)),\quad \epsilon=E_0, \tag{23}$$

are solutions of Eq. (18a).

The solution of nonhomogeneous Eq. (18b) can be found in a form similar to the form of the inhomogeneity $c_\epsilon(\boldsymbol{p},t)$, so that we present $f_\epsilon^{(r)}(\boldsymbol{p},t)$ in the form

$$f_\epsilon^{(r)}(\boldsymbol{p},t)=2\pi\sum_s\int\frac{e^{iS_\epsilon(\boldsymbol{k};t,t_s')}}{\sqrt{2\pi i\alpha_s}}\tau(\boldsymbol{p},\boldsymbol{k},t)f_\epsilon^{(s)}(\boldsymbol{k},t_s')d\boldsymbol{k}, \tag{24}$$

where $\tau(\boldsymbol{p},\boldsymbol{k};t)$ is a smooth function, whose form should be found. It should be noticed, that the form of function (24) is found in agreement with the conception of low-frequency (or adiabatic) approximation. Indeed, the low-frequency approximation assumes that the exponential $e^{iS_\epsilon(\boldsymbol{k};t,t_s')}$ is a rapidly oscillating function, while the functions associated with an atomic potential are considered as smooth functions of their variables. The function $\tau(\boldsymbol{p},\boldsymbol{k},t)$ can be related with an atomic potential [see Eqs. (26)–(28) below] and be considered as a smooth function.

With known $f_\epsilon^{(r)}(\tilde{\boldsymbol{k}},t'')$, we estimate the integral over time in Eq. (18b) by taking into account the contribution from the vicinity of the upper limit ($t''=t$):[2]

$$-i\int_{-\infty}^{t}e^{iS_\epsilon(\tilde{\boldsymbol{k}};t,t'')}f_\epsilon^{(r)}(\boldsymbol{k},t'')dt'' \approx 4\pi\sum_s\int\frac{e^{iS_\epsilon(\boldsymbol{k};t,t')}}{\sqrt{2\pi i\alpha_s}}f_\epsilon^{(s)}(\boldsymbol{k},t')\frac{\tau(\tilde{\boldsymbol{k}},\boldsymbol{k};t)}{\boldsymbol{K}^2(t)-\widetilde{\boldsymbol{K}}^2(t)+i0}d\boldsymbol{k}, \tag{25}$$

where $\widetilde{\boldsymbol{K}}(t)=\tilde{\boldsymbol{k}}+\boldsymbol{A}(t)$. In obtaining Eq. (25), the following two-term expansion near $t''=t$ is taken into account:

$$S_\epsilon(\tilde{\boldsymbol{k}};t,t'')+S_\epsilon(\boldsymbol{k};t'',t_s') \approx S_\epsilon(\boldsymbol{k};t,t_s')+\frac{t-t''}{2}[\boldsymbol{K}^2(t)-\widetilde{\boldsymbol{K}}^2(t)+i0],$$

[2]The contribution from corresponding saddle points of the integrand in Eq. (18b) is negligible, since it is suppressed by the contribution of saddle points of $f_\epsilon^{(r)}(\tilde{\boldsymbol{k}},t'')$.

and an infinitesimal is added to ensure convergence at the lower limit.

Substituting $f_\epsilon^{(r)}(\boldsymbol{p},t)$ in the form (24) into Eq. (18b) and taking into account Eq. (25), we obtain the integral equation for function $\tau(\boldsymbol{p},\boldsymbol{k};t)$:

$$\tau(\boldsymbol{p},\boldsymbol{k};t) = u(\boldsymbol{p}-\boldsymbol{k}) + 2\int \frac{u(\boldsymbol{p}-\tilde{\boldsymbol{k}})\tau(\tilde{\boldsymbol{k}},\boldsymbol{k};t)}{\boldsymbol{K}^2(t)-\widetilde{\boldsymbol{K}}^2(t)+i0}\,d\tilde{\boldsymbol{k}}. \quad (26)$$

It is easy to check that Eq. (26) coincides with the equation for half-shell $T$ matrix $T(\boldsymbol{p},\boldsymbol{k}) \equiv T(\boldsymbol{p},\boldsymbol{k};k^2/2)$ [32] with momenta $\boldsymbol{p}$ and $\boldsymbol{k}$ replaced by the instantaneous field-induced momenta,

$$\tau(\boldsymbol{p},\boldsymbol{k};t) = T(\boldsymbol{P}(t),\boldsymbol{K}(t)). \quad (27)$$

Indeed, the equation for the off-shell $T$ matrix $T(\boldsymbol{p},\boldsymbol{k};\varepsilon)$, defined for arbitrary $\varepsilon$ [32],

$$T(\boldsymbol{p},\boldsymbol{k};\varepsilon) = u(\boldsymbol{p}-\boldsymbol{k}) + \int \frac{u(\boldsymbol{p}-\tilde{\boldsymbol{k}})T(\tilde{\boldsymbol{k}},\boldsymbol{k};\varepsilon)}{\varepsilon-\tilde{\boldsymbol{k}}^2/2+i0}\,d\tilde{\boldsymbol{k}}, \quad (28)$$

turns to Eq. (26) for $\varepsilon = \boldsymbol{K}^2(t)/2, \boldsymbol{k} = \boldsymbol{K}(t)$, and $\boldsymbol{p} = \boldsymbol{P}(t)$. For $\varepsilon = p^2/2 = k^2/2$, the on-shell $T$-matrix determines the electron elastic scattering amplitude: $\mathcal{A}(\boldsymbol{p},\boldsymbol{k}) = -4\pi^2 T(\boldsymbol{p},\boldsymbol{k};\varepsilon)$.

Taking into account Eqs. (23), (27), and (24), we obtain the final result for $f_\epsilon^{(r)}(\boldsymbol{p},t)$:

$$f_\epsilon^{(r)}(\boldsymbol{p},t) = 2\pi\sum_s \int \frac{e^{iS_{E_0}(\boldsymbol{k};t,t_s')}}{\sqrt{2\pi i\,\alpha_s}} \times T(\boldsymbol{P}(t),\boldsymbol{K}(t))f_{E_0}^{(0)}(\boldsymbol{K}(t_s'))d\boldsymbol{k}. \quad (29)$$

From Eq. (29) is clearly seen that the effects of electron-core interaction are described by two factors: the function $f_{E_0}^{(0)}(\boldsymbol{K}(t_s'))$ is the laser-modified atomic bound state, taken at some time $t_s'$, and the $T$ matrix $T(\boldsymbol{P}(t),\boldsymbol{K}(t))$ describes the electron scattering on the atomic potential with the momentum exchange from $\boldsymbol{K}(t)$ to $\boldsymbol{P}(t)$ at the time $t$. Thus, the function $f_\epsilon^{(r)}(\boldsymbol{p},t)$ represents the "rescattering" approximation for $f_\epsilon(\boldsymbol{p},t)$ and plays a key role for the description of rescattering effects in the amplitudes of laser-induced processes.

### B. Low-frequency approximation for the detachment amplitude

Taking into account the low-frequency result for the function $f_\epsilon(\boldsymbol{p},t)$ [see Eqs. (13), (23), and (29)], we present the detachment amplitude (12) as the sum of two terms:

$$\mathcal{A}(\boldsymbol{p}_n) = \mathcal{A}^{(s)}(\boldsymbol{p}_n) + \mathcal{A}^{(r)}(\boldsymbol{p}_n), \quad (30)$$

where

$$\mathcal{A}^{(s)}(\boldsymbol{p}_n) = -\frac{4\pi^2}{\mathcal{T}}\int_{-\mathcal{T}/2}^{\mathcal{T}/2} dt e^{iS_{p_n}(t)} f_{E_0}^{(0)}(\boldsymbol{P}_n(t)), \quad (31a)$$

$$\mathcal{A}^{(r)}(\boldsymbol{p}_n) = -\frac{(2\pi)^3}{\mathcal{T}}\sum_s \int_{-\mathcal{T}/2}^{\mathcal{T}/2} dt e^{iS_{p_n}(t)} \int d\boldsymbol{k}\frac{e^{iS_{E_0}(\boldsymbol{k},t,t_s')}}{\sqrt{2\pi i\alpha_s}} \times f_{E_0}^{(0)}(\boldsymbol{K}(t_s'))T(\boldsymbol{P}_n(t),\boldsymbol{K}(t)). \quad (31b)$$

Amplitude (31a) is used for the description of low-energy photoelectrons and known as the Keldysh amplitude [6–8] or the strong field approximation (SFA) amplitude [44,45], which has been an attractive subject of research for more than 50 years (see, e.g., Refs. [46–49]). High-energy (or rescattering [50]) electrons are described by the amplitude (31b). This part of detachment amplitude is usually considered within the improved SFA [51,52] (see also Refs. [3,5,9]), which takes into account atomic potential effects perturbatively. In the low-frequency approximation, we show that all dynamic atomic potential effects can be combined into the $T$ matrix element (see also Ref. [37]).

In the low-frequency approximation, amplitudes (31a) and (31b) can be estimated within the saddle-point method. We shall focus our further analysis on the rescattering amplitude (31b). The saddle-point integration in Eq. (31b) over $\boldsymbol{k}$ gives the amplitude $\mathcal{A}^{(r)}(\boldsymbol{p}_n)$ in the form

$$\mathcal{A}^{(r)}(\boldsymbol{p}_n) = \frac{(2\pi)^4}{\mathcal{T}}\sum_s \int_{-\mathcal{T}/2}^{\mathcal{T}/2} \frac{e^{i\mathcal{S}(\boldsymbol{p}_n;t,t_s')}}{\sqrt{\alpha(t,t_s')}(t-t_s')^{3/2}} \times f_{E_0}^{(0)}(\boldsymbol{K}'(t,t_s'))T(\boldsymbol{P}_n(t),\boldsymbol{K}(t,t_s'))dt, \quad (32)$$

where

$$\mathcal{S}(\boldsymbol{p}_n;t,t') = \frac{1}{2}\int^t \boldsymbol{P}_n^2(\xi)d\xi - E_0 t' - \frac{1}{2}\int_{t'}^t \left(\boldsymbol{A}(\xi) - \frac{1}{t-t'}\int_{t'}^t \boldsymbol{A}(\tau)d\tau\right)^2 d\xi, \quad (33a)$$

$$\alpha(t,t') = \boldsymbol{K}'(t,t')\cdot\boldsymbol{F}(t'), \quad (33b)$$

$$\boldsymbol{K}'(t,t') = \boldsymbol{A}(t') - \frac{1}{t-t'}\int_{t'}^t \boldsymbol{A}(\tau)d\tau, \quad (33c)$$

$$\boldsymbol{K}(t,t') = \boldsymbol{A}(t) - \frac{1}{t-t'}\int_{t'}^t \boldsymbol{A}(\tau)d\tau, \quad (33d)$$

and $t_s'$ obeys the equation [see Eq. (17) with $\epsilon = E_0$ and $\boldsymbol{k} = -\int_{t_s'}^t \boldsymbol{A}(\xi)d\xi/(t-t_s')$]:

$$\boldsymbol{K}'^2(t,t_s') = 2E_0, \quad t_s' \equiv t_s'(t). \quad (34)$$

The temporal integral in Eq. (32) can be estimated within the method suggested in Refs. [25,42], which is based on the assumptions that the condition of adiabaticity is fulfilled, i.e., $\mathrm{Im}\,\omega t_s' \ll 1$, and the dynamics of the electron in the continuum is governed by classical laws, thereby allowing one to consider time $t$ as a real one at the evaluation of integral. Details of derivations are presented in Appendix B and we proceed with the final result.

Our final result for the ATD amplitude is expressed in terms of *real* ionization time $\overline{t_j'}$ and rescattering time $\overline{t_j}$, which obey the system of transcendental equations:

$$\boldsymbol{K}_j'\cdot\dot{\boldsymbol{K}}_j' = 0, \quad (35a)$$

$$\frac{\boldsymbol{P}_n^2(\overline{t_j})}{2} - \frac{\boldsymbol{K}_j^2}{2} - \Delta\mathcal{E}_j = 0, \quad (35b)$$

$$\Delta\mathcal{E}_j = -\frac{(\kappa^2+\boldsymbol{K}_j'^2)}{(\overline{t_j}-\overline{t_j'})\mathcal{F}_j^2}\left[\frac{\boldsymbol{K}_j\cdot\boldsymbol{K}_j'}{\overline{t_j}-\overline{t_j'}} - \frac{\boldsymbol{F}_j'\cdot(\boldsymbol{K}_j-\boldsymbol{K}_j')}{2}\right], \quad (35c)$$

where $\kappa = \sqrt{2|E_0|}$ and

$$\boldsymbol{K}'_j = \boldsymbol{K}'(\overline{t_j}, \overline{t'_j}), \quad \dot{\boldsymbol{K}}'_j = \frac{\partial \boldsymbol{K}'(\overline{t_j}, \overline{t'_j})}{\partial \overline{t'_j}}, \quad \boldsymbol{K}_j = \boldsymbol{K}(\overline{t_j}, \overline{t'_j}),$$

$$\mathcal{F}_j = \sqrt{\boldsymbol{F}'^{\,2}_j - \boldsymbol{K}'_j \cdot \dot{\boldsymbol{F}}'_j}, \quad \boldsymbol{F}'_j = \boldsymbol{F}(\overline{t'_j}), \quad \dot{\boldsymbol{F}}'_j = \frac{\partial \boldsymbol{F}(\overline{t'_j})}{\partial \overline{t'_j}}.$$

Equation (35a) shows that the electron liberates into the continuum at the moment, which ensures the minima of electron energy at the time $\overline{t'_j}$. Equation (35b) shows the condition at which the variation of action (33a) in time $t$ equals zero. If correction $\Delta\mathcal{E}_j$ is neglected in Eq. (35b), this equation shows the conservation law for kinetic energies of incoming and rescattering electrons, however, this correction (although it is small) is nonzero due to (i) correlation between ionization and rescattering times assigned by Eq. (35a) and (ii) nonzero binding energy $I_p$ and kinetic energy of the electron at the moment $\overline{t'_j}$.

With the set of times $\overline{t_j}$ and $\overline{t'_s}$, the amplitude $\mathcal{A}^{(r)}(\boldsymbol{p}_n)$ can be presented as a sum of partial amplitudes, $a_j^{(r)}(\boldsymbol{p}_n)$, (see details in Appendix B):

$$\mathcal{A}^{(r)}(\boldsymbol{p}_n) = -\frac{4\pi^2}{\mathcal{T}} \sum_j a_j^{(r)}(\boldsymbol{p}_n), \tag{36}$$

$$a_j^{(r)}(\boldsymbol{p}_n) = a_j^{(\mathrm{tun})} a_j^{(\mathrm{prop})} T(\boldsymbol{P}_n(\overline{t_j}), \boldsymbol{K}_j), \tag{37}$$

where each term will be discussed in turn.

*Tunneling factor*, $a_j^{(\mathrm{tun})}$, is given by the Keldysh-like detachment amplitude in the adiabatic approximation [53,54]:

$$a_j^{(\mathrm{tun})} = 2\pi C_{\kappa l} \frac{e^{-\frac{\varkappa_j^3}{3\mathcal{F}_j}}}{\sqrt{\varkappa_j \mathcal{F}_j}} Y_{lm}(\boldsymbol{e}_j), \tag{38}$$

where $\varkappa_j = \sqrt{\kappa^2 + \boldsymbol{K}'^{\,2}_j}$, $\boldsymbol{e}_j = (\boldsymbol{K}'_j + i\dot{\boldsymbol{K}}'_j \Delta_j)/\kappa$ is the unit (up to the order of $\Delta_j^2$) complex vector, and $\Delta_j = \varkappa_j/\mathcal{F}_j$.

*Propagation factor*, $a_j^{(\mathrm{prop})}$, describes the dynamics of the electron in the continuum and is given by the expression

$$a_j^{(\mathrm{prop})} = \frac{e^{i\mathcal{S}(\boldsymbol{p}_n; \overline{t_j}, \overline{t'_j})}}{(\overline{t_j} - \overline{t'_j})^{3/2} \sqrt{2\pi i \beta_j}}, \tag{39}$$

where the action $\mathcal{S}(\boldsymbol{p}_n; \overline{t_j}, \overline{t'_j})$ is determined by Eq. (33a) and

$$\beta_j = \boldsymbol{F}_j \cdot [\boldsymbol{K}_j - \boldsymbol{P}_n(\overline{t_j})] + \frac{\boldsymbol{K}_j^2}{\overline{t_j} - \overline{t'_j}}, \quad \boldsymbol{F}_j = \boldsymbol{F}(\overline{t_j}). \tag{40}$$

We should emphasize that for those energies, which ensure zeros of $\beta_j$ (the caustic point [56–59]), the presented approach is not applicable and special treatment should be applied at the caustic points [see Eq. (41) below].

The last factor in Eq. (37) is given by the corresponding $T$-matrix element for two continuum states with initial momentum $\boldsymbol{K}_j$ and final momentum $\boldsymbol{P}_n(\overline{t_j})$. Although the energies of these two states differ by the amount $\Delta\mathcal{E}_j$ [see Eq. (35c)], due to its smallness, for the most practical cases the half-shell $T$-matrix element can be replaced by the on-shell one, determining the elastic scattering amplitude, $\mathcal{A}$, i.e., approximating

$$\boldsymbol{K}_j \approx \mathcal{K}_j \equiv |\boldsymbol{P}_n(\overline{t_j})| \frac{\boldsymbol{K}_j}{|\boldsymbol{K}_j|},$$

$$T(\boldsymbol{P}_n(\overline{t_j}), \boldsymbol{K}_j) \approx -\frac{1}{4\pi^2} \mathcal{A}(\boldsymbol{P}_n(\overline{t_j}), \mathcal{K}_j).$$

Since $\Delta\mathcal{E}_j$ is of the order of $\kappa^2$ and $\boldsymbol{P}_n(\overline{t_j})^2 \propto F^2/\omega^2$, $\boldsymbol{K}_j^2 \propto F^2/\omega^2$, the inaccuracy in the aforementioned replacement is of the order of a squared Keldysh parameter, which for the adiabatic case is much less than unity: $\Delta\mathcal{E}_j/\boldsymbol{P}_n^2(\overline{t_j}) \propto \omega^2\kappa^2/F^2 \ll 1$.

The analytical result, Eq. (37), for partial detachment amplitude is found in agreement with suggested three-step scenario (ionzation, propagation, and scattering) for the forming of high energy electrons [50]. Moreover, this result explicitly shows how the many-electron effects can be implemented into the detachment amplitude: through the asymptotic coefficient $C_{\kappa l}$ in the tunneling factor (38) and the $T$-matrix element. Also, besides many-electron calculations of $C_{\kappa l}$, this coefficient can be also calculated by matching the inner part of initial state (for instance, calculating within Slater-type orbitals) with the asymptotics (21) (see, e.g., Ref. [55]).

The result, Eq. (39), for the propagation factor is valid for those values of photoelectron momentum $\boldsymbol{p}_n$, which ensure a real solution of the system (35). However, there is a set of photoelectron momenta directed along $\boldsymbol{p}_n$, $\boldsymbol{p}_0 = p_0\hat{\boldsymbol{p}}_n$, whose infinitesimal shift may change a number of *real* solutions of the system (35). These momenta define positions of caustics in the momentum distribution of photoelectrons. Therefore, the propagation factor (39) depends on a number of suitable real solutions, whose sudden changes lead to unphysical steplike (or discontinuity) behavior in the momentum distributions or ATD spectra. This unphysical behavior can be excluded by considering more precisely the partial amplitudes, $a_j^{(r)}(\boldsymbol{p}_n)$, near the caustic. As our analysis shows, these amplitudes exponentially decrease behind the caustic (see Appendix C) and the smooth transition between two regions (before and beyond the caustic) is analytically described by the Airy function [23,24,39]. To take into account the exponential tails of "classically forbidden" partial amplitudes (it means that they cannot be described in terms of real trajectories) in the total amplitude, we should extract from the sum (36) a pair of partial amplitudes, which corresponds to two almost merged trajectories, and replace this pair by a "transient" amplitude, $\tilde{a}_j^{(r)}$ (see Appendix C). The amplitude $\tilde{a}_j^{(r)}$ has the same analytic structure as $a_j^{(r)}$ (see Appendix C) and may be obtained as follows: (i) by substituting $\overline{t'_j} \to t'_0$, $\overline{t_j} \to t_0$ in the expression for the tunneling factor and the $T$ matrix, where $t'_0$ and $t_0$ are ionization and rescattering times for an extreme classical trajectory corresponding to a given caustic; (ii) by replacing the propagation factor (39) by

$$\tilde{a}_j^{(\mathrm{prop})} = \frac{e^{i\mathcal{S}(\boldsymbol{p}_0; t_0, t'_0)}}{(t_0 - t'_0)^{3/2}} \left(\frac{2}{\gamma_0}\right)^{1/3} \mathrm{Ai}\left[-\frac{\mathcal{D}}{4}\left(\frac{2}{\gamma_0}\right)^{4/3}\right], \tag{41}$$

where $\mathrm{Ai}(x)$ is the Airy function. For a given direction of the photoelectron momentum, $\boldsymbol{p}_0 = p_0\hat{\boldsymbol{p}}_n$, the magnitudes of $p_0$, $t_0$, and $t_0'$ can be found from the system (35) (with substitution $\boldsymbol{p}_n \to \boldsymbol{p}_0$) supplemented by the additional equation:

$$\beta_j = 0. \tag{42}$$

With the obtained $p_0$, $t_0$, and $t_0'$, the parameters $\mathcal{D}$ and $\gamma_0$ in the argument of the Airy function in Eq. (41) are found in accordance with Eqs. (C6b), (C12) from Appendix C.

To take into account depletion effects of an initial state, we introduce coefficient $\mathcal{P}_j$, which effectively accounts depletion effects in the adiabatic limit [21]:

$$\mathcal{A}^{(r)}(\boldsymbol{p}_n) = \frac{1}{2\pi\mathcal{T}}\sum_j \mathcal{P}_j a_j^{(r)}(\boldsymbol{p}_n), \tag{43}$$

$$\mathcal{P}_j \equiv \mathcal{P}(\overline{t_j'}), \quad \mathcal{P}(t) = \exp\left[-\frac{1}{2}\int_{-\infty}^{t}\Gamma(\boldsymbol{F}(\tau))d\tau\right], \tag{44}$$

where $\Gamma(F)$ is the detachment rate[3] for an initial bound state in a DC field with strength $F = |\boldsymbol{F}(\tau)|$. Since $\Gamma(F)$ is a positive function, $\mathcal{P}(t)$ is a decreasing function of time and thus partial amplitudes $a_j^{(r)}(\boldsymbol{p}_n)$ are suppressed for those $j$, which correspond to $\mathcal{P}_j \ll 1$ (or $\max[\Gamma(|\boldsymbol{F}(t)|)]\mathcal{T} \gtrsim 1$). This suppression destroys the comblike structure in ATD spectra, which results from coherent interference of partial amplitudes. In the oppositive case of $\max[\Gamma(|\boldsymbol{F}(t)|)]\mathcal{T} \ll 1$, this factor is not important and can be neglected, so that the comblike structure of ATD spectrum shows up.

The extension to the case of short pulses can be fulfilled with the procedure suggested in Refs. [24,43]. This procedure results in the formal replacements in the ATD amplitude (36) and supplemented equations: $\boldsymbol{p}_n \to \boldsymbol{p}$, where $\boldsymbol{p}$ is the momentum of an ionized electron with energy $E_p = \boldsymbol{p}^2/2$; factor $1/(2\pi\mathcal{T}) \to 1/(2\pi)^2$. As a result, we obtain the double differential probability, $\mathcal{P}^{(r)}(p)$, for photoelectrons:

$$\mathcal{P}^{(r)}(\boldsymbol{p}) = \frac{d^3W}{dE_p d\Omega_{\boldsymbol{p}}} = \frac{p}{(2\pi)^3}\left|\sum_j \mathcal{P}_j a_j^{(r)}(\boldsymbol{p})\right|^2, \tag{45}$$

where $\Omega_{\boldsymbol{p}}$ is the solid angle of a detached electron, $W$ is the detachment probability. [Note that the momentum distribution, $d^3W/d^3\boldsymbol{p}$, follows from Eq. (45) by dividing $d^3W/dE_p d\Omega_{\boldsymbol{p}}$ by the factor $p$.]

## IV. NUMERICAL RESULTS

### A. Comparison with TDSE results

We check the accuracy of our analytical result (45) by comparison with the numerical solution of TDSE (see details in Appendix D). The TDSE is solved for a Yukawa potential

$$U(r) = -U_0\frac{e^{-\alpha r}}{r}, \tag{46}$$

where $U_0 = 1.908$, $\alpha = 1$. The potential (46) supports a single bound $s$-state with the binding energy $I_p = 0.5$ a.u. and the asymptotic coefficient in Eq. (21) is $C_{\kappa l=0} = 2.73$. In Fig. 1, we compare the elastic electron scattering cross section and the phase of the scattering amplitude for the potential (46) with their counterparts for the Coulomb potential $-U_0/r$. For backscattering (scattering angle more than 90°), cross sections for the Yukawa and the Coulomb potentials are close to each other for larger energies, since for these energies the most contribution is given by small distances, where two potentials are close to each other. However, the phases of scattering amplitude as a function of the electron energy show significant difference between Yukawa and Coulomb potentials (see bottom panels in Fig. 1). This difference may cause changes in the interference of partial amplitudes (37) for the Coulomb field, so that Coulomb effects crucially modify the interference pattern in the momentum distribution of ionized electrons, and these effects will be considered elsewhere.

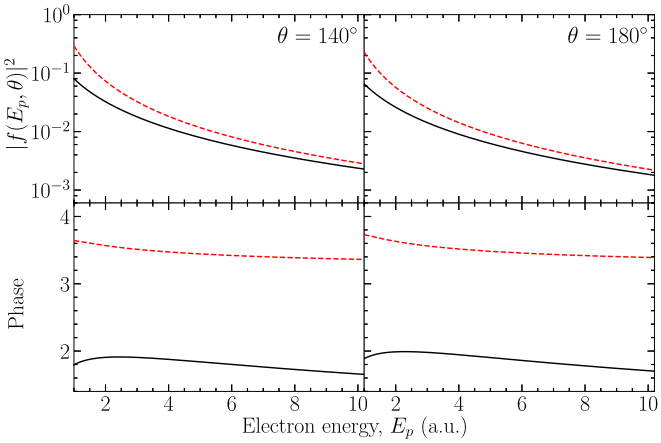


FIG. 1. Energy dependence of the electron scattering cross section (upper panels) and the phase of the scattering amplitude (bottom pannels) for Yukawa [see Eq. (46)] (black solid lines) and Coulomb, $-U_0/r$, (red dashed lines) potentials. Scattering angles are marked in the figure.

In the first numerical example for ATD, we consider a linearly polarized pulse with $\cos^2$ shape for the vector potential:

$$\boldsymbol{A}(t) = -\hat{\boldsymbol{z}}\frac{F}{\omega}\cos^2\left(\frac{\pi t}{\tau}\right)\sin(\omega t + \phi), \tag{47}$$

where $F$ is the peak strength, $\tau$ is the total duration of the laser pulse, $\omega$ and $\phi$ are the carrier frequency and phase. In Fig. 2, we present the angle-energy resolved distribution of photoelectrons for a laser pulse with peak intensity $I = cF^2/(8\pi) = 1.5\times10^{14}$ W/cm$^2$, $\lambda = 2\pi c/\omega = 1.3$ $\mu$m, $\phi = \pi/2$, and total duration $\tau = 26$ fs (six laser cycles for the total duration). Since for the linearly polarized laser pulse the angular distribution is symmetric with respect to the polarization axis (i.e., the ATD yields are the same for angles $\theta$ and $2\pi - \theta$, where $0 < \theta < \pi$), we present the numerical TDSE results in the upper part of the figure, while the lower part corresponds to the analytical result (45).

In Fig. 3, we present ATD spectra extracted from Fig. 2 at six different angles. The sharp spikes (see dotted lines in Fig. 3) correspond to caustic energies, $E_i^{(c)}$, [56,60], at

[3]For practical calculations we use the standard tunneling formula for the detachment rate [see, e.g., Eq. (4) in Ref. [7]].

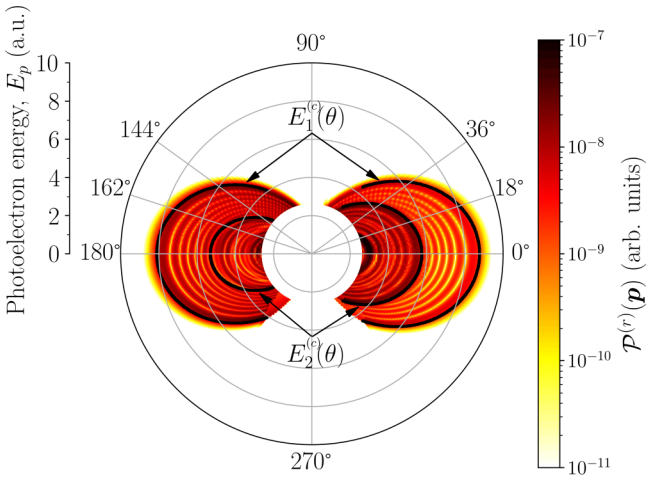


FIG. 2. Color-coded angle-energy distribution of photoelectrons for the potential (46) and a laser pulse (47) with peak intensity $I = cF^2/(8\pi) = 1.5 \times 10^{14}$ W/cm$^2$, wavelength $\lambda = 1.3$ $\mu$m, $\phi = \pi/2$, and total duration $\tau = 26$ fs. The upper part of the figure presents TDSE results, the lower part of the figure is calculated with the analytical result (45). Solid black lines show the dependence of the caustic energy on the angle $\theta$.

which the second (or higher order) derivative of classical action is zero. For ATD, these caustic energies depend on the angle between momentum $\boldsymbol{p}$ and polarization vector $\hat{\boldsymbol{z}}$ (see solid black lines in Fig. 2). As we pointed out in Sec. III B, near caustic energies a special theoretical treatment for ATD amplitude is necessary [23,24,39,60], since such energies determine thresholds at which some classically allowed (i.e., real) closed trajectories disappear.[4] For example, for $E > E_1^{(c)}(\theta)$ (see Fig. 3), there are no closed classically-allowed trajectories and the corresponding ATD amplitude is determined by an exponentially decreasing behavior [see Eq. (C14b) in Appendix C]. However, for $E_2^{(c)}(\theta) < E < E_1^{(c)}(\theta)$ one pair of trajectories (long and short) is allowed and leads to large-scale oscillations [61,62] [see Figs. 3(a)–3(c)]. Extra pairs of classical trajectories contribute to the ATD amplitude as the photoelectron energy decreases and crosses caustic energies. Extra trajectories [or extra roots of Eq. (35)] modify large-scale oscillations by superposing fine-scale oscillations on the large-scale structures [see, e.g., Figs. 3(d)–3(f)] [24,63]. It should be noted that exponentially decreasing partial amplitude may interfere with other oscillatory behaved amplitudes leading to an oscillatory pattern on the slope of the ATD amplitude (see, e.g., the black line in Fig. 3(b) for 5.25 a.u. $< E_p <$ 6 a.u.). The angle-energy distribution in Fig. 2 shows the remarkable left-right asymmetry, which is well understood within the rescattering model for a short laser pulse [4,5]. According to this model, (i) the electron is ejected by a laser field from the atom at the moment $t_i$, (ii) the field returns the electron back to the atomic core at the moment $t_f$, and (iii) the electron get backscattered. The two last steps are happened near the maximum of the vector potential, while the first one appears near the maximum of the electric field. For a monochromatic field, all these events repeat periodically every half cycle, thereby forming a symmetric distribution of the ionized electrons (we note, the

[4]Mathematically this means that the number of roots of system (35) differs above and below a caustic energy.

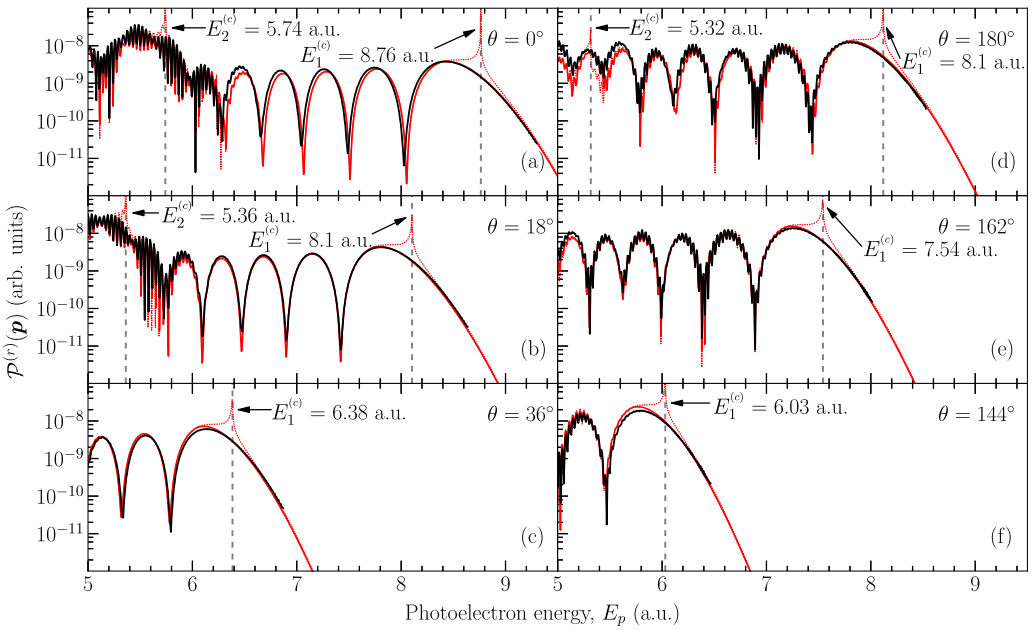


FIG. 3. ATD spectra for the potential (46) and six angles $\theta$ (extracted from Fig. 2), where $\theta$ is the angle between momentum of photoelectron $\boldsymbol{p}$ and polarization vector $\hat{\boldsymbol{z}}$. Vertical dashed lines mark caustic positions for the given angles $\theta$. Solid black lines: TDSE results; solid red lines: the analytical result (45) [with appropriate behavior of the propagation factor near the caustic]; dotted red lines: the asymptotic behavior of ATD yield near the caustic [see Eq. (C14b) for the propagation factor near the caustic].

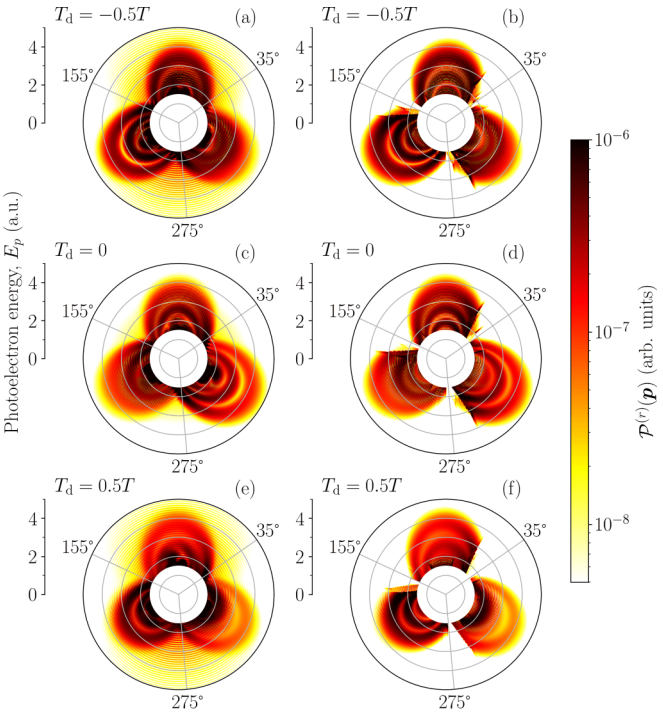


FIG. 4. Momentum distribution of photoelectrons for the potential (46) in the bicircular field (48) with $I = cF^2/(8\pi) = 10^{14}$ W/cm$^2$, $\omega = 1.55$ eV, $N_1 = 2$, $N_2 = 4$, $T_d = -0.5T_d$ (a), (b), $T_d = 0$ (c), (d), $T_d = 0.5T$ (e), (f). Left panels: TDSE results; right panels: presented analytical result. Gray lines divide momentum distribution into three sectors (see text for details).

electrons ionized on the "positive" half cycle contribute to the right hemisphere, while the electrons produced by "negative" half cycle contribute to the left hemisphere). For a short laser pulse having an envelope $f(t)$, this periodicity is breaking down, thus the distribution does not hold the left-right symmetry. This rescattering mechanism also leads to the asymmetric positions of caustics for two $\pi$-connected ATD spectra [cf. panels (a) and (d), (b) and (e), and (c) and (f) in Fig. 3].

We present the further comparison with numerical TDSE results for the time-delayed few-cycle bicircular field, whose electric component is parametrized in the form:

$$\boldsymbol{F}(t) = -\frac{\partial \boldsymbol{A}(t)}{\partial t} = -\frac{\partial^2 \boldsymbol{R}(t)}{\partial t^2}, \tag{48a}$$

$$\boldsymbol{R}(t) = \boldsymbol{R}_1(t) + \boldsymbol{R}_2(t - T_d), \tag{48b}$$

$$\boldsymbol{R}_i(t) = \frac{F}{\omega_i^2} f_i(t)(\boldsymbol{e}_x \cos\omega_i t + \eta_i \boldsymbol{e}_y \sin\omega_i t), \tag{48c}$$

$$f_i(t) = e^{-2\ln 2\, t^2/\tau_i^2}, \tag{48d}$$

where each component $i = 1, 2$ of the field $\boldsymbol{F}(t)$ has the strength $F$, carrier frequency $\omega_i$ ($\omega_1 = \omega_2/2 = \omega$), ellipticity $\eta_i$ ($\eta_1 = -\eta_2 = 1$), duration $\tau_i = 2\pi N_i/\omega$ (full width at half maximum of the intensity), number of cycles $N_i$, and $T_d$ is the time delay between the two components (if $T_d$ is negative, the $2\omega$-pulse precedes the $\omega$ pulse). We perform calculations for $I = cF^2/(8\pi) = 10^{14}$ W/cm$^2$, $\omega = 1.55$ eV, $N_1 = 2, N_2 = 4$, $T_d = -0.5T$, where $T = 2\pi/\omega$ [see Figs. 4(a) and 4(b)], $T_d = 0$ [see Figs. 4(c) and 4(d)], $T_d = 0.5T$ [see Figs. 4(e) and 4(f)], and potential (46). In Figs. 4 and 5, we present comparisons for the bicircular field, which show perfect agreement between TDSE and analytic results. Discrepancies at small energies are caused by contribution of the Keldysh part of detachment amplitude [see Eq. (31a)] omitted in this work.

### B. Enhancement of ATD yield with time-delayed laser pulses

We analyze below the modification of ATD spectra by changing the time delay between two circularly polarized pulses. If components with carrier frequencies $\omega$ and $2\omega$ in Eq. (48) are monochromatic, the time delay may be related to the relative phase between $\omega$ and $2\omega$ components. In this case, the momentum distribution of photoelectrons in the polarization plane is given by a perfect three-lobe distribution [64–67] and changing the relative phase leads to the kinematic rotation of the whole momentum distribution on the angle $\Delta\varphi = 2T_d\omega/3$ [66]. Therefore, the time delay (or relative phase) between two components does not affect dynamically the momentum distribution of photoelectrons for the case of monochromatic components of a bicircular field.

For the time-delayed pulsed bicircular field, the above-discussed symmetry in the momentum distribution does not hold and a variation of the time delay between two circularly polarized pulses leads to dynamical changes in the momentum distribution of photoelectrons. To demonstrate these changes we introduce the integrated ATD yield:

$$\mathcal{Y} = \int_{\varphi_{\min}}^{\varphi_{\max}} d\varphi \int_{E_{\min}}^{E_{\max}} dE_p \mathcal{P}^{(r)}(\boldsymbol{p}), \tag{49}$$

where the vector $\boldsymbol{p}$ has zero projection on the $z$ axis [$\boldsymbol{p} = (p\cos\varphi, p\sin\varphi, 0)$] and $\varphi$ is the angle between vectors $\boldsymbol{e}_x$ and $\boldsymbol{p}$. In our calculations for laser parameters as those in Fig. 4, we set $E_{\min} = 2.0$ a.u. and $E_{\max} = 6.0$ a.u., while angles $\varphi_{\min}$ and $\varphi_{\max}$ divide the polarization plane into three equal sectors of angle $2\pi/3$: for the first sector $\varphi_{\min} = -85^\circ + \Delta\varphi$ and $\varphi_{\max} = 35^\circ + \Delta\varphi$ (we mark this yield as $\mathcal{Y}_1$); for second sector $\varphi_{\min} = 35^\circ + \Delta\varphi$ and $\varphi_{\max} = 155^\circ + \Delta\varphi$ (we mark this yield as $\mathcal{Y}_2$); for third sector $\varphi_{\min} = 155^\circ + \Delta\varphi$ and $\varphi_{\max} = 275^\circ + \Delta\varphi$ (we mark this yield as $\mathcal{Y}_3$). We notice, that in order to take into account the kinematic rotation of the momentum distribution, edge angles $\varphi_{\min}$ and $\varphi_{\max}$ are defined with an extra term $\Delta\varphi$ [see Figs. (4)]. In Fig. 6, we present the time-delay dependence of $\mathcal{Y}_i$ [see Fig. 6(a)] and the total yield [see Fig. 6(b)]:

$$\mathcal{Y}_{\text{tot}} = \sum_{i=1}^{3} \mathcal{Y}_i. \tag{50}$$

For the time delays, which do not provide a significant overlap of two circularly polarized pulses (c.f., $|T_d| > 1.5T$ in Fig. 6), the corresponding yields $\mathcal{Y}_i$ gradually decrease with increasing $|T_d|$ due to the suppression of the rescattering mechanism in producing high-energy electrons. For small time delays, it would be intuitively expected that yields $\mathcal{Y}_i$ should be a smooth function of time delay, which is maximized at $T_d = 0$, i.e., at a complete overlapping of two pulses. However, our calculations show: (i) yields $\mathcal{Y}_i$ demonstrate oscillatory behavior for the time delays, which ensure well overlapping of two circularly polarized pulses (see the range

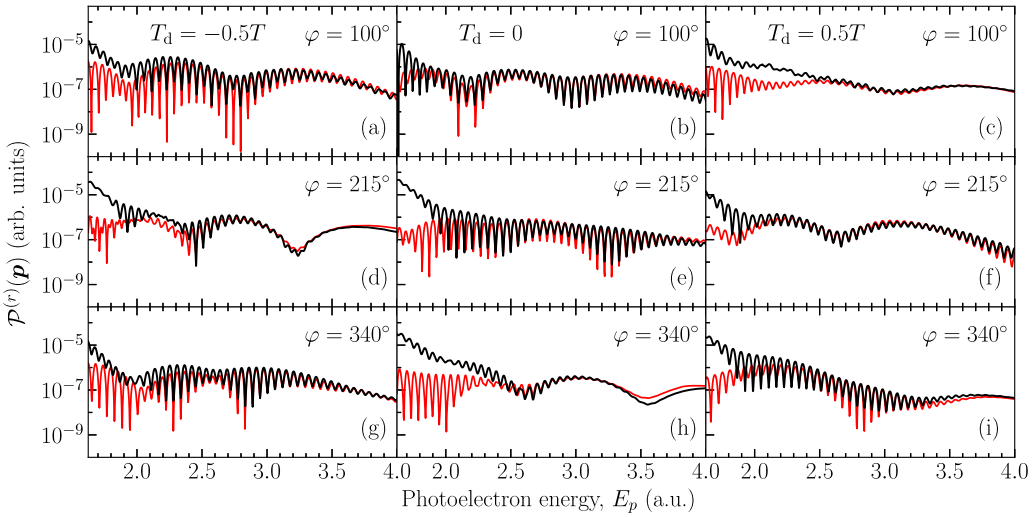


FIG. 5. Comparison of ATD spectra for given detachment angles. TDSE and analytical results are extracted from Fig. 4. Solid black lines: TDSE results; solid red lines: present analytic result (45). Laser parameters are the same as in Fig. 4.

$|T_d| < 1.5T$ in Fig. 6); (ii) yields $\mathcal{Y}_i$ are maximized not for $T_d = 0$. Similar results have been observed previously for high harmonic generation yield in the time-delayed bicircular field [41,42]. Although oscillation patterns are similar for all three integrated yields, nevertheless, the magnitude of corresponding oscillations is different (note that for the bicircular field with monochromatic components $\mathcal{Y}_1 = \mathcal{Y}_2 = \mathcal{Y}_3 = \text{const}$).

All these counterintuitive effects can be attributed to the differences between the subcycle dynamics for a bicircular field with monochromatic components and a time-delayed bicircular pulse. In contrast to the latter case, the dynamics of an electron in the bicircular field with monochromatic components is the same every one-third of the laser period $T = 2\pi/\omega$, thereby forming the threefold symmetric momentum distribution [64–66]. The momentum distribution for the $2\pi/3$ sector is mostly formed by those electrons, for which the process of rescattering[5] is realized during the one-third of the laser period and repeated through the period $T$. However, for the short time-delayed bicircular pulse, each rescattering event is individual due to the absence of periodicity in the pulsed field, so that magnitudes and phases of contributing partial amplitudes differ significantly from their counterparts for the bicircular field with monochromatic components. This subcycle difference in rescattering events leads to the oscillation pattern observed in Fig. 6. (Detailed analysis of the modification of the observed oscillation pattern in the integrated yield by the long-range Coulomb potential will be discussed somewhere else.) We notice, that for bicircular field with monochromatic components, interference of partial amplitudes can be reduced to the product of ATD rate and a comblike function with peaks separated by the photon energy.

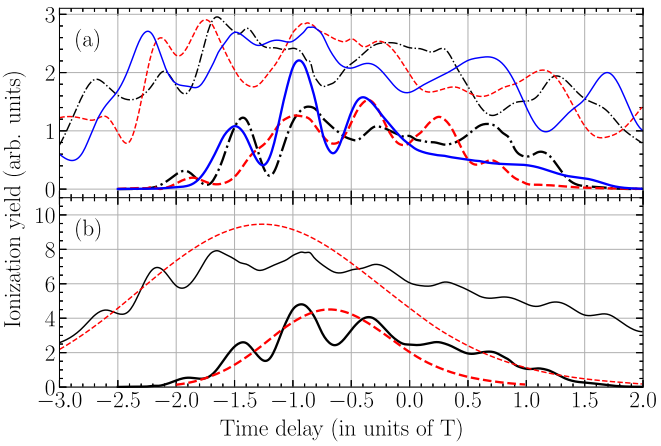


FIG. 6. The time-delay dependence of integrated ATD yields $\mathcal{Y}_i$ ($i = 1, 2, 3$) and $\mathcal{Y}_{\text{tot}}$ [see Eqs. (49), (50) and text for details] and integrated tunneling factor $\mathcal{I}_{\text{tun}}$ [see Eq. (51)]. (a) Black thick dash-dotted line: $\mathcal{Y}_1$, $N_1 = 2$, $N_2 = 4$; red thick dashed line: $\mathcal{Y}_2$, $N_1 = 2$, $N_2 = 4$; blue thick solid line: $\mathcal{Y}_3$, $N_1 = 2$, $N_2 = 4$; black thin dash-dotted line: $\mathcal{Y}_1$, $N_1 = 4$, $N_2 = 8$; red thin dashed line: $\mathcal{Y}_2$, $N_1 = 4$, $N_2 = 8$; blue thin solid line: $\mathcal{Y}_3$, $N_1 = 4$, $N_2 = 8$. (b) Black thick solid line: $\mathcal{Y}_{\text{tot}}$, $N_1 = 2$, $N_2 = 4$; black thin solid line: $\mathcal{Y}_{\text{tot}}$, $N_1 = 4$, $N_2 = 8$; red thick dashed line: $\mathcal{I}_{\text{tun}}$, $N_1 = 2$, $N_2 = 4$; red thin dashed line: $\mathcal{I}_{\text{tun}}$, $N_1 = 4$, $N_2 = 8$. The laser intensity and frequencies are the same as in Fig. 4. Laser field is parameterized by Eq. (48).

To show that the ionization factor also depends on the time delay, in Fig. 6 we present the integrated tunneling factor, $\mathcal{I}_{\text{tun}}$, as a function of the time delay:

$$\mathcal{I}_{\text{tun}} = \sum_j \int_0^{2\pi} d\varphi \int_{E_1}^{E_2} dE_p \left| \mathcal{P}_j a_j^{(\text{tun})} \right|^2, \tag{51}$$

where $j$ is the index of contributing trajectory. Similarly to the ATD yield (50), the dependence of $\mathcal{I}_{\text{tun}}$ on the time delay is mostly determined by the degree of overlapping of two pulses. For long pulses, the ionization factor becomes more sloppy and its dependence is mostly given by the depletion factors, which lead to a smooth decreasing of $\mathcal{I}_{\text{tun}}$ in the range of well overlapping of two pulses. Our result for integrated ionization

[5]Rescattering consists of the releasing of an atomic electron from the target near the maximum of the electric field lobe and its returning to the atomic core with subsequent scattering near the minimum of the electric field at the neighboring lobe.

factor explicitly shows that interference patterns in Fig. 6 are the result of a mutual interference between different partial ATD amplitudes and cannot be caused by the appearance (or disappearance) of closed classical trajectories.

## V. SUMMARY AND OUTLOOK

In this work, we have analyzed ATD in the low-frequency limit for a laser field with an arbitrary waveform. The developed low-frequency approximation is based on the QQES approach, which properly treats the dynamics of a valence electron in both a short-range binding potential and an intense periodic laser field. In the low-frequency limit, we have shown explicitly that the detachment amplitude can be expressed in terms of the $T$ matrix for collision problems, thereby providing a rigorous mathematical justification of heuristically suggested parametrization for ATD amplitude [37] (see also Ref. [22] in [40]). We have presented the rescattering part of the ATD amplitude in terms of partial amplitudes, which can be associated with closed classical electron trajectories. Such a trajectory corresponds to the gained particular electron energy at the rescattering, which ensures a given final energy of photoelectron. For a given momentum of photoelectron, this closed trajectory may be parametrized within the real starting (or ionization) and finishing (or rescattering) time. In terms of these times, the partial ATD amplitudes can be factorized in three terms corresponding to the three steps in forming of high-energy photoelectron spectrum: the tunneling term describes ionization step; the propagation term describes a quasiclassical motion along a closed trajectory, and the $T$ matrix (or the amplitude of elastic electron scattering) describes interaction of a continuum electron with binding potential. Our analysis shows that each partial ATD amplitude can be associated with the classical trajectories only inside of some surface in $\boldsymbol{p}$ space, which separates classically allowed and classically forbidden regions. This surface (caustic surface) determines those momenta of photoelectrons, for which two closed classical trajectories merge into a single extreme trajectory. We have shown that near this surface, the partial amplitude can be approximately described in terms of the Airy function and ionization and rescattering times for the extreme trajectory. We note that this "transient" asymptotics of ATD amplitude in terms of the Airy function smoothly sews together the oscillating asymptotic in the classically allowed region with exponentially decreasing behavior in the classically forbidden region.

We have checked the accuracy of the developed low-frequency approximation for rescattering ATD amplitude by comparison with the numerical solution of TDSE for the Yukawa potential supporting a single bound state. Calculations have been performed for linearly polarized pulse and the time-delayed bicircular field. In both cases, excellent agreement between low-frequency approximation and TDSE results is observed. This agreement is achieved by applying the "transient" asymptotics for partial ATD amplitudes, which allows us to avoid the nonphysical singularity in the ATD yield near the caustic surface.

The analytical treatment of ATD has been used to study the dependence of ATD yield on the time delay between two components of the bicircular field. We have shown that (i) the ATD yield may be maximized by changing the time delay between the two few-cycle circularly polarized pulses; (ii) the maximum of ATD yield for the case of two short pulses is achieved for nonzero time delay, which corresponds to partial overlapping of two pulses; (iii) the dependence of ATD yield is not a smooth function of a time delay and exhibits a regular oscillation pattern. All these effects originate from the deviation of the electric field of the bicircular pulse from the perfect three-lobe structure (realized for the case of monochromatic components of the bicircular field) and disappear as the duration of each component increases.

Finally, we note that above-discussed effects may be significantly modified by the long-range Coulomb field, so that a special treatment is necessary for the inclusion of Coulomb effects at the analysis of ionization of neutral atoms or positive ions. Indeed, the previous study shows that Coulomb effects may lead, e.g., to a rotation of the momentum distribution [68,69]. Moreover, the Coulomb field may affect on the interference of different partial amplitudes due to inducing a specific additional phase to these amplitudes and change the dependence of ionization yield on the time delay. The extension of results of this paper with inclusion of Coulomb field effects can be performed within quasiclassical (or phase) perturbation theory (see, e.g., Refs. [70–72]) and will be published elsewhere.

## ACKNOWLEDGMENTS

This work was supported in part by the Russian Science Foundation through Grant No. 18-12-00476 (numerical calculations and theory development), by the Ministry of Education and Science of the Russian Federation through the Project No. FZGU-2020-0035 (N.L.M.), by the National Natural Science Foundation of China (NSFC) under Grant No. 11725416, and by the National Key R&D Program of China under Grant No. 2018YFA0306302 (L.G. and L.P.). Authors thank S. Popruzhenko and V. Tulsky for fruitful discussions. M.V.F. acknowledges the financial support of the Russian Foundation for Basic Research (Grant No. 20-32-70213).

## APPENDIX A: ASYMPTOTIC BEHAVIOR OF THE QQES WAVE FUNCTION

In this Appendix, we present details of derivation of the asymptotic behavior of QQES wave function at large distances. For this purpose, the quasienergy state wave function (5) of the free electron in a laser field is convenient to represent in the form

$$\chi_{\boldsymbol{p}}(\boldsymbol{r},t) = e^{i\boldsymbol{p}\cdot\boldsymbol{R}(\boldsymbol{r},t)+i\alpha(\boldsymbol{r},t)}, \tag{A1}$$

where

$$\boldsymbol{R}(\boldsymbol{r},t) = \boldsymbol{r} - \int^{t} \boldsymbol{A}(\tau)d\tau, \tag{A2a}$$

$$\alpha(\boldsymbol{r},t) = \boldsymbol{r}\cdot\boldsymbol{A}(t) - \int^{t} [A^2(\tau)/2 - u_p]d\tau. \tag{A2b}$$

Substituting Eq. (A1) into Eq. (7) and integrating in directions of momentum $\boldsymbol{q}$, we obtain the Green's function in the

form

$$G(\boldsymbol{r},t;\boldsymbol{r}',t') = -\frac{1}{(2\pi)^2}\frac{e^{i(\alpha-\alpha')}}{|\boldsymbol{R}-\boldsymbol{R}'|} \times \int_{-\infty}^{\infty} dq\, q\, e^{iq|\boldsymbol{R}-\boldsymbol{R}'|-i(q^2/2+u_p)(t-t')}, \quad \text{(A3)}$$

where $\boldsymbol{R}\equiv\boldsymbol{R}(\boldsymbol{r},t)$, $\boldsymbol{R}'\equiv\boldsymbol{R}(\boldsymbol{r}',t')$, $\alpha\equiv\alpha(\boldsymbol{r},t)$, $\alpha'\equiv\alpha(\boldsymbol{r}',t')$. Substituting Eq. (A3) into Eq. (2) and taking into account the equality

$$\frac{1}{2\pi}\frac{e^{i(\alpha-\alpha')+iq|\boldsymbol{R}-\boldsymbol{R}'|}U(r')\Phi_\epsilon(\boldsymbol{r}',t')}{|\boldsymbol{R}-\boldsymbol{R}'|} = e^{i\alpha}\sum_n e^{-in\omega_\tau t'}\frac{1}{2\pi\mathcal{T}}\int_{-\mathcal{T}/2}^{\mathcal{T}/2}\frac{e^{-i\alpha''+iq|\boldsymbol{R}-\boldsymbol{R}''|}}{|\boldsymbol{R}-\boldsymbol{R}''|} \times U(r')\Phi_\epsilon(\boldsymbol{r}',t'')e^{in\omega_\tau t''}dt'',$$

$$\alpha'' \equiv \alpha(\boldsymbol{r}',t''), \quad \boldsymbol{R}''\equiv\boldsymbol{R}(\boldsymbol{r}',t''),$$

we rewrite Eq. (2) as

$$\Phi_\epsilon(\boldsymbol{r},t) = \frac{e^{i\alpha}}{2\pi}\int_{-\infty}^{t}dt'\int_{-\infty}^{\infty}dq\,q\,e^{-i(q^2/2+u_p-\epsilon)(t-t')} \times \sum_n C_n(q;\boldsymbol{r},t)e^{-in\omega_\tau t'}, \quad \text{(A4)}$$

where

$$C_n(q;\boldsymbol{r},t) = -\frac{1}{2\pi\mathcal{T}}\int_{-\mathcal{T}/2}^{\mathcal{T}/2}e^{in\omega_\tau t''}dt''\int d\boldsymbol{r}' \times \frac{e^{iq|\boldsymbol{R}-\boldsymbol{R}''|-i\alpha''}}{|\boldsymbol{R}-\boldsymbol{R}''|}U(r')\Phi_\epsilon(\boldsymbol{r}',t''). \quad \text{(A5)}$$

The functions $C_n(q;\boldsymbol{r},t)$ exponentially decrease with increasing $|q|$ in the complex plane of $q$ for $\mathrm{Im}\,q>0$, so that the integration in Eq. (A4) can be carried out first in time $t'$ and then in $q$ by using the residue integration method

$$\int_{-\infty}^{\infty}dq\,qC_n(q;\boldsymbol{r},t)\int_{-\infty}^{t}dt'e^{-i(q^2-p_n^2)(t-t')/2} = -2i\int_{-\infty}^{\infty}dq\,\frac{qC_n(q;\boldsymbol{r},t)}{q^2-p_n^2-i0} = 2\pi C_n(p_n;\boldsymbol{r},t), \quad \text{(A6)}$$

where $p_n=\sqrt{2(\epsilon+n\omega_\tau-u_p)}$. As a result, we obtain the following representation for the QQES wave function:

$$\Phi_\epsilon(\boldsymbol{r},t) = e^{i\alpha(\boldsymbol{r},t)}\sum_n C_n(p_n;\boldsymbol{r},t)e^{-in\omega_\tau t}. \quad \text{(A7)}$$

To consider the limit of large distances in Eq. (A7), we use in Eq. (A5) the well-known asymptotics for $|\boldsymbol{R}|\gg|\boldsymbol{R}'|$,

$$\frac{e^{ip_n|\boldsymbol{R}-\boldsymbol{R}'|}}{|\boldsymbol{R}-\boldsymbol{R}'|}\approx\frac{e^{ip_n|\boldsymbol{R}|-i\boldsymbol{p}_n\cdot\boldsymbol{R}'}}{|\boldsymbol{R}|}, \quad \boldsymbol{p}_n = p_n\boldsymbol{R}/|\boldsymbol{R}|,$$

and obtain the expression for the QQES wave function in the form of outgoing spherical waves at large distances:

$$\Phi_\epsilon(\boldsymbol{r},t)|_{r\to\infty}\simeq e^{i\alpha(\boldsymbol{r},t)}\sum_n\mathcal{A}_n(\boldsymbol{p}_n)\frac{e^{ip_n|\boldsymbol{R}(\boldsymbol{r},t)|-in\omega_\tau t}}{|\boldsymbol{R}(\boldsymbol{r},t)|}, \quad \text{(A8)}$$

where the coefficients $\mathcal{A}_n(\boldsymbol{p}_n)$ for $n\geqslant[(u_p-\epsilon)/\omega_\tau]$ are the ATD amplitudes:

$$\mathcal{A}_n(\boldsymbol{p}_n) = -\frac{1}{2\pi\mathcal{T}}\int_{-\mathcal{T}/2}^{\mathcal{T}/2}dt\,e^{in\omega_\tau t} \times \int d\boldsymbol{r}\,\chi^*_{\boldsymbol{p}_n}(\boldsymbol{r},t)U(r)\Phi_\epsilon(\boldsymbol{r},t). \quad \text{(A9)}$$

## APPENDIX B: EVALUATION OF THE AMPLITUDE (32)

The temporal integral in Eq. (32) can be estimated analytically under two assumptions: (i) the imaginary part of time $t_s'$ is essentially smaller than the characteristic period of a laser pulse, $T=2\pi/\omega$, i.e., $\mathrm{Im}\,t_s'/T\ll1$ (or $\omega\mathrm{Im}\,t_s'\ll1$); (ii) the integration in $t$ can be carried out over the real axis, i.e., quantum effects negligibly contribute to the electron dynamics into the continuum. Within these assumptions, $t_s'$ can be presented as $t_s'=\overline{t_s'}+i\Delta_s$, where $\overline{t_s'}$ and $\Delta_s$ are real. Owing to the smallness of $\Delta_s$, Eqs. (34) and scalars $\mathcal{S}(\boldsymbol{p}_n;t,t_s')$, $\alpha(t_j,t_s')$ [see Eq. (33)] can be expanded in the formal series in $\Delta_s$ (see, e.g., Ref. [25]) and expressed in terms of real times $\overline{t_s'}$:

$$\mathcal{S}(\boldsymbol{p}_n;t,t_s') \approx \mathcal{S}(\boldsymbol{p}_n;t,\overline{t_s'}) + i\frac{\varkappa^3(t,\overline{t_s'})}{3\mathcal{F}(t,\overline{t_s'})}, \quad \text{(B1a)}$$

$$\alpha(t,t_s') \approx \varkappa(t,\overline{t_s'})\mathcal{F}(t,\overline{t_s'}), \quad \text{(B1b)}$$

$$\varkappa(t,\overline{t_s'}) = \sqrt{\kappa^2+\boldsymbol{K}'(t,\overline{t_s'})^2}, \quad \text{(B1c)}$$

$$\mathcal{F}(t,\overline{t_s'}) = \sqrt{\boldsymbol{F}^2(\overline{t_s'})-\boldsymbol{K}'(t,\overline{t_s'})\cdot\dot{\boldsymbol{F}}(\overline{t_s'})}, \quad \text{(B1d)}$$

$$T(\boldsymbol{P}_n(t),\boldsymbol{K}(t,t_s')) \approx T(\boldsymbol{P}_n(t),\boldsymbol{K}(t,\overline{t_s'})) + i\Delta(t,\overline{t_s'})\frac{\boldsymbol{K}'(t,\overline{t_s'})}{t-\overline{t_s'}} \cdot\frac{\partial T(\boldsymbol{P}_n(t),\boldsymbol{K})}{\partial\boldsymbol{K}}\bigg|_{\boldsymbol{K}=\boldsymbol{K}(t,\overline{t_s'})}, \quad \text{(B1e)}$$

$$\dot{\boldsymbol{F}}(t) = \frac{\partial\boldsymbol{F}(t)}{\partial t}, \quad \Delta(t,\overline{t_s'}) = \frac{\varkappa(t,\overline{t_s'})}{\mathcal{F}(t,\overline{t_s'})}, \quad \text{(B1f)}$$

where $\overline{t_s'}$ is found from equation (see details in Ref. [25]):

$$\boldsymbol{K}'(t,\overline{t_s'})\cdot\dot{\boldsymbol{K}}'(t,\overline{t_s'}) = 0,$$

$$\dot{\boldsymbol{K}}'(t,\overline{t_s'}) = \frac{\partial\boldsymbol{K}'(t,\overline{t_s'})}{\partial\overline{t_s'}} = -\boldsymbol{F}(\overline{t_s'}) + \frac{\boldsymbol{K}'(t,\overline{t_s'})}{t-\overline{t_s'}}. \quad \text{(B2)}$$

We should emphasize that $\overline{t_s'}$ and $\Delta_s$ are single-valued functions of $t$, so that $\varkappa$, $\mathcal{F}$, $\mathcal{S}(\boldsymbol{p}_n;t,\overline{t_s'})$ are well-defined single-valued functions. Substituting approximate expressions from Eq. (B1) into Eq. (32) and applying saddle-point estimate for the temporal integral, we obtain

$$\mathcal{A}^{(r)}(\boldsymbol{p}_n) = \frac{1}{2\pi\mathcal{T}}\sum_j a_j^{(\mathrm{tun})}a_j^{(\mathrm{prop})}T(\boldsymbol{P}_n(\overline{t_j}),\boldsymbol{K}_j), \quad \text{(B3)}$$

where

$$a_j^{(\mathrm{tun})} = \frac{1}{\sqrt{2\pi i}}\frac{e^{-\frac{\varkappa_j^3}{3\mathcal{F}_j}}}{\sqrt{\varkappa_j\mathcal{F}_j}}f_{E_0}^{(0)}(\boldsymbol{K}_j'+i\Delta_j\dot{\boldsymbol{K}}_j'), \quad \text{(B4a)}$$

$$\varkappa_j = \varkappa(\overline{t_j}, \overline{t'_j}), \quad \mathcal{F}_j = \mathcal{F}(\overline{t_j}, \overline{t'_j}),$$

$$a_j^{(\mathrm{prop})} = \frac{e^{i\mathcal{S}(\boldsymbol{p}_n;\overline{t_j},\overline{t'_j})}}{(\overline{t_j}-\overline{t'_j})^{3/2}\sqrt{\beta_j}}, \tag{B4b}$$

$$\beta_j = \boldsymbol{F}_j \cdot [\boldsymbol{K}_j - \boldsymbol{P}_n(\overline{t_j})] + \frac{\boldsymbol{K}_j^2}{\overline{t_j}-\overline{t'_j}}, \tag{B4c}$$

$$\boldsymbol{K}'_j = \boldsymbol{K}'(\overline{t_j}, \overline{t'_j}), \quad \dot{\boldsymbol{K}}'_j = \dot{\boldsymbol{K}}'(\overline{t_j}, \overline{t'_j}), \tag{B4d}$$

$$\boldsymbol{K}_j = \boldsymbol{K}(\overline{t_j}, \overline{t'_j}), \quad \boldsymbol{F}_j = \boldsymbol{F}(\overline{t_j}), \tag{B4e}$$

and the pair of times $\overline{t_j}$ and $\overline{t'_j}$ is found from system of the transcendental equations:

$$\boldsymbol{K}'_j \cdot \dot{\boldsymbol{K}}'_j = 0, \tag{B5a}$$

$$\frac{\boldsymbol{P}_n^2(\overline{t_j})}{2} - \frac{\boldsymbol{K}_j^2}{2} = \Delta\mathcal{E}_j, \tag{B5b}$$

$$\Delta\mathcal{E}_j = -\frac{\left(\kappa^2 + \boldsymbol{K}_j'^2\right)}{(\overline{t_j}-\overline{t'_j})\mathcal{F}_j^2}\left[\frac{\boldsymbol{K}_j \cdot \boldsymbol{K}'_j}{\overline{t_j}-\overline{t'_j}} - \frac{\boldsymbol{F}'_j \cdot (\boldsymbol{K}_j - \boldsymbol{K}'_j)}{2}\right], \quad \boldsymbol{F}'_j = \boldsymbol{F}(\overline{t'_j}). \tag{B5c}$$

We emphasize that roots of the system (B5) should be separated into two groups (corresponding to conditions $\beta_j > 0$ and $\beta_j < 0$) and applied separately for calculation of photoelectron spectra with particular geometry of the detached electron: for instance, for linear polarization these conditions correspond to detachment (ionization) in the right ($\beta_j > 0$) or the left ($\beta_j < 0$) hemisphere.

## APPENDIX C: EVALUATION OF AN INTEGRAL NEAR THE CAUSTIC

Let us consider an integral

$$\mathcal{I}(\alpha) = \int_{-\infty}^{\infty} g(t)\exp\left[i\Phi(\alpha,t)\right]dt, \tag{C1}$$

where $g(t)$, $\Phi(\alpha,t)$ are smooth functions and $\alpha$ is a parameter. The saddle points of the integrand in Eq. (C1) are given by solution of the equation

$$\Phi'_t(\alpha,t) = 0, \quad \Phi'_t(\alpha,t) = \frac{\partial\Phi(\alpha,t)}{\partial t}, \tag{C2}$$

and the integral (C1) within the saddle-point approximation takes the form:

$$\mathcal{I}(\alpha) = \sum_{t_{\mathrm{sp}}} g(t_{\mathrm{sp}})\sqrt{\frac{2\pi i}{\Phi''_{tt}(\alpha,t_{\mathrm{sp}})}}\exp\left[i\Phi(\alpha,t_{\mathrm{sp}})\right]. \tag{C3}$$

Our goal is to evaluate the integral (C1) near the caustic

$$\Phi'_t(\alpha_0,t_0) = 0, \quad \Phi''_{tt}(\alpha_0,t_0) = 0, \tag{C4}$$

where $\Phi''_{tt} = \partial^2\Phi(\alpha,t)/\partial t^2$, $\alpha_0$ is the caustic value of $\alpha$, $t_0$ is the saddle point at the caustic. First, we expand function $\Phi'_t(\alpha,t)$ near the caustic in series over $\alpha$ and $t$:

$$\Phi'_t(\alpha,t) \approx \gamma_0\frac{(t-t_0)^2}{2} + \beta_0(\alpha-\alpha_0)(t-t_0) + \Delta_0 = \frac{\gamma_0}{2}\left[t - t_0 + \frac{\beta_0}{\gamma_0}(\alpha-\alpha_0)\right]^2 + \Delta_0 - \frac{\beta_0^2(\alpha-\alpha_0)^2}{2\gamma_0}, \tag{C5}$$

where

$$\gamma_0 = \left.\frac{\partial^3\Phi(\alpha,t)}{\partial t^3}\right|_{\substack{t=t_0\\ \alpha=\alpha_0}}, \quad \beta_0 = \left.\frac{\partial^3\Phi(\alpha,t)}{\partial\alpha\,\partial t^2}\right|_{\substack{t=t_0\\ \alpha=\alpha_0}},$$

$$\Delta_0 = \delta_1(\alpha-\alpha_0) + \delta_2\frac{(\alpha-\alpha_0)^2}{2},$$

$$\delta_1 = \left.\frac{\partial^2\Phi(\alpha,t)}{\partial\alpha\,\partial t}\right|_{\substack{t=t_0\\ \alpha=\alpha_0}}, \quad \delta_2 = \left.\frac{\partial^3\Phi(\alpha,t)}{\partial\alpha^2\partial t}\right|_{\substack{t=t_0\\ \alpha=\alpha_0}}.$$

We notice that terms $\Phi'_t(\alpha_0,t_0)$ and $\Phi''_{tt}(\alpha_0,t_0)$ fall out from expansion (C5), because of Eq. (C4). Using Eq. (C5), we obtain the expansion of the saddle point $t_{\mathrm{sp}}$ and $\Phi(\alpha,t_{\mathrm{sp}})$ near the caustic

$$t_{\mathrm{sp}} \approx t_0 + \delta t_{\mathrm{sp}}, \quad \delta t_{\mathrm{sp}} = -\frac{\beta_0}{\gamma_0}\delta\alpha \pm \frac{\sqrt{\mathcal{D}}}{\gamma_0}, \tag{C6a}$$

$$\mathcal{D} = \beta_0^2\delta\alpha^2 - 2\gamma_0\Delta_0, \quad \delta\alpha = \alpha - \alpha_0, \tag{C6b}$$

$$\Phi''_{tt}(\alpha,t_{\mathrm{sp}}) \approx \pm\sqrt{\mathcal{D}}, \tag{C6c}$$

$$\Phi(\alpha,t_{\mathrm{sp}}) = \Phi(\alpha_0+\delta\alpha, t_0+\delta t_{\mathrm{sp}}) \approx \Phi(\alpha,t_0) \mp \frac{\mathcal{D}^{3/2}}{3\gamma_0^2}. \tag{C6d}$$

With the expansion (C6), the integral (C1) near the caustic takes the form

$$\mathcal{I}(\alpha) = \mathcal{C}\begin{cases} e^{i\frac{\pi}{4}-i\frac{\mathcal{D}^{3/2}}{3\gamma_0^2}} + e^{-i\frac{\pi}{4}+i\frac{\mathcal{D}^{3/2}}{3\gamma_0^2}} & \mathcal{D} > 0 \\ e^{-\frac{|\mathcal{D}|^{3/2}}{3\gamma_0^2}} & \mathcal{D} < 0 \end{cases}, \tag{C7}$$

$$\mathcal{C} = \sqrt{2\pi}\,g(t_0)e^{i\Phi(\alpha,t_0)}|\mathcal{D}|^{-1/4}. \tag{C8}$$

The expression (C7) represents two asymptotics of the Airy function, so that $J(\alpha)$ may be approximated by an analytic function at any $\mathcal{D}$:

$$\mathcal{I}(\alpha) = 2\sqrt{\pi}\,g(t_0)\left(\frac{2}{\gamma_0}\right)^{1/3}\mathrm{Ai}\left[-\frac{\mathcal{D}}{4}\left(\frac{2}{\gamma_0}\right)^{4/3}\right]e^{i\Phi(\alpha,t_0)}. \tag{C9}$$

We notice that in Eq. (C7) only terms of the lowest order in $\sqrt{\delta\alpha}$ for $\delta t_{\mathrm{sp}}$ have been taken into account. The result (C9) can be also derived straightforwardly from the integral (C1) approximating the function $\Phi(t)$ by a cubic polynomial (see details in the Appendix of Ref. [24]).

The result (C7) allows one to estimate the partial detachment amplitude $a_j^{(r)}$ [see Eq. (37)] near the caustic energy. In this case, the function $\Phi(\alpha,t)$ is given by the classical action $\mathcal{S}(\boldsymbol{p}_n;t,t'(t))$ in Eq. (33a), in which the $t$-dependence of $t'(t)$ is implicitly determined by Eq. (35a) and the parameter $\alpha$ is given by $p_n$. Thereby the system of three transcendental

equations, Eq. (35a) and Eqs. (C4), for the "caustic" ionization time, $t_0'$, rescattering time, $t_0$, and $p_n$ is

$$\boldsymbol{K}_0' \cdot \dot{\boldsymbol{K}}_0' = 0, \tag{C10a}$$

$$\frac{\boldsymbol{P}_n^2(t_0)}{2} - \frac{\boldsymbol{K}_0^2}{2} - \Delta\mathcal{E}_0 = 0, \tag{C10b}$$

$$\boldsymbol{F}_0 \cdot [\boldsymbol{K}_0 - \boldsymbol{P}_n(t_0)] + \frac{\boldsymbol{K}_0^2}{t_0 - t_0'} = 0,$$

$$\Delta\mathcal{E}_0 = -\frac{\left(\kappa^2 + \boldsymbol{K}_0'^2\right)}{(t_0 - t_0')\mathcal{F}_0^2}\left[\frac{\boldsymbol{K}_0 \cdot \boldsymbol{K}_0'}{t_0 - t_0'} - \frac{\boldsymbol{F}_0' \cdot (\boldsymbol{K}_0 - \boldsymbol{K}_0')}{2}\right], \tag{C10c}$$

where

$$\boldsymbol{K}_0' \equiv \boldsymbol{K}'(t_0, t_0'), \quad \boldsymbol{K}_0 \equiv \boldsymbol{K}(t_0, t_0'), \quad \dot{\boldsymbol{K}}_0' \equiv \dot{\boldsymbol{K}}'(t_0, t_0'),$$

$$\boldsymbol{F}_0 = \boldsymbol{F}(t_0), \quad \boldsymbol{F}_0' = \boldsymbol{F}(t_0'), \quad \dot{\boldsymbol{F}}_0' = \frac{\partial \boldsymbol{F}(t_0')}{\partial t_0'},$$

$$\mathcal{F}_0 = \sqrt{\boldsymbol{F}_0'^2 - \boldsymbol{K}_0' \cdot \dot{\boldsymbol{F}}_0'}.$$

Equations (C10a) and (C10b) coincide with Eqs. (35a) and (35b) and determine the ionization and rescattering times for a given $\boldsymbol{p}_n$, while Eq. (C10c) corresponds to Eq. (42) in the main text and determines the "caustic" value $p_0$ of the photoelectron momentum for a given direction $\hat{\boldsymbol{p}}_n$. The caustic rescattering energy $E^{(c)}$, corresponding to $p_0$, is given by

$$E^{(c)} = \frac{\boldsymbol{K}_0^2}{2} + \Delta\mathcal{E}_0 = \frac{1}{2}[\boldsymbol{p}_0 + \boldsymbol{A}(t_0)]^2, \tag{C11}$$

where $\boldsymbol{p}_0 = p_0\hat{\boldsymbol{p}}_n$.

Straightforward calculations of $\Delta_0$, $\beta_0$, and $\gamma_0$ give

$$\Delta_0 = \frac{1}{2}[\boldsymbol{p}_n + \boldsymbol{A}(t_0)]^2 - E^{(c)}, \tag{C12a}$$

$$\beta_0\delta\alpha = \boldsymbol{F}_0 \cdot (\boldsymbol{p}_n - \boldsymbol{p}_0), \tag{C12b}$$

$$\gamma_0 = \dot{\boldsymbol{F}}_0 \cdot [\boldsymbol{K}_0 - \boldsymbol{P}_n(t_0)] - 3\frac{\boldsymbol{F}_0 \cdot \boldsymbol{P}_n(t_0)}{t_0 - t_0'}. \tag{C12c}$$

As a result, the partial amplitude $\tilde{a}_j^{(r)}$ near the caustic may be written in the form similar to Eq. (36):

$$\tilde{a}_j^{(r)}(\boldsymbol{p}_n) = a_j^{(\mathrm{tun})}\tilde{a}_j^{(\mathrm{prop})}T(\boldsymbol{P}_n(t_0), \boldsymbol{K}_0), \tag{C13}$$

where

$$a_j^{(\mathrm{tun})} = \frac{e^{-\frac{\varkappa_0^3}{3\mathcal{F}_0}}}{\sqrt{\varkappa_0\mathcal{F}_0}} f_{E_0}^{(0)}(\boldsymbol{K}_0' + i\Delta_j\dot{\boldsymbol{K}}_0'), \tag{C14a}$$

$$\tilde{a}_j^{(\mathrm{prop})} = \frac{1}{\sqrt{(t_0 - t_0')^3\pi}}\left(\frac{2}{\gamma_0}\right)^{1/3}\mathrm{Ai}\left[-\frac{\mathcal{D}}{4}\left(\frac{2}{\gamma_0}\right)^{4/3}\right]$$

$$\approx \mathcal{C}\begin{cases} e^{\pm i\left(\frac{\pi}{4} - \frac{\mathcal{D}^{3/2}}{3\gamma_0^2}\right)} & \mathcal{D} > 0 \\ e^{-\frac{|\mathcal{D}|^{3/2}}{3\gamma_0^2}} & \mathcal{D} < 0 \end{cases}, \tag{C14b}$$

$$\mathcal{C} = \frac{e^{i\mathcal{S}_0}}{(t_0 - t_0')^{3/2}\sqrt{2\pi\sqrt{|\mathcal{D}|}}}, \tag{C14c}$$

$$\mathcal{S}_0 = \frac{1}{2}\int^{t_0} \boldsymbol{P}_n^2(\tau)d\tau - E_0 t_0'$$

$$- \frac{1}{2}\int_{t_0'}^{t_0}\left(\boldsymbol{A}(\xi) - \frac{1}{t_0 - t_0'}\int_{t_0'}^{t_0}\boldsymbol{A}(\tau)d\tau\right)^2 d\xi, \tag{C14d}$$

where $\mathcal{D}$ is given by Eq. (C6b) with notations (C12), $\varkappa_0 = \sqrt{\kappa^2 + \boldsymbol{K}_0'^2}$, and the sign "+" (or "−") in Eq. (C14b) should be chosen if $\tilde{a}_j^{(r)}$ corresponds to the short (or long) trajectory.

## APPENDIX D: NUMERIC SOLUTION OF TDSE

For the numerical solution of TDSE, we use the velocity gauge and the dipole approximation for electron-laser interaction

$$i\dot{\Psi}(\boldsymbol{r}, t) = H\Psi(\boldsymbol{r}, t), \quad H = -\frac{\nabla^2}{2} + U(r) - i\boldsymbol{A}(t) \cdot \nabla, \tag{D1}$$

where $U(r)$ is the atomic potential, $\boldsymbol{A}(t)$ is the vector potential of a laser pulse. The desired time-dependent wave function is expanded in terms of spherical harmonics $Y_{lm}(\hat{\boldsymbol{r}})$:

$$\Psi(\boldsymbol{r}, t) = \frac{1}{r}\sum_{l=0}^{l_{\max}}\sum_{m=-l}^{m=l}\psi_{lm}(r, t)Y_{lm}(\hat{\boldsymbol{r}}). \tag{D2}$$

The radial coordinate $r$ is discretized by the finite element discrete variable representation [73]. The whole coordinate space of $r$ is divided into many finite elements. Gauss–Lobatto quadratures of order 8 are used as basis functions in every finite element. In this work, we use the Arnoldi propagator [74] to carry out the evolution of the wave function from the initial state. To save the computational time and reduce the reflection effect, the splitting scheme [75] is used for the wave function $\Phi(\boldsymbol{r}, t)$:

$$\Psi = \Psi_{\mathrm{inner}} + \Psi_{\mathrm{outer}} = M\Psi + (1 - M)\Psi. \tag{D3}$$

The wave function is split by a mask function $M$

$$M(r) = \frac{1}{1 + \exp\left(\frac{r - r_c}{r_w}\right)}, \tag{D4}$$

where $r_c = 0.5r_{\max}$ and $r_w = 0.03r_{\max}$, with $r_{\max}$ being the maximum of the $r$ grid. The outer part of $\Psi(\boldsymbol{r}, t)$, $\Psi_{\mathrm{outer}}$, is separated every one-third cycle of the laser pulse at time $t_i$, which is then projected to scattering states and analytically propagated till the end of pulse $t_f$ by the Volkov propagator,

$$U_{\mathrm{Volkov}}(t_f, t_i) = \exp\left[-iE(t_f - t_i) - i\int_{t_i}^{t_f}\boldsymbol{p} \cdot \boldsymbol{A}(\tau)d\tau\right]. \tag{D5}$$

When the laser pulse is off, the residual wave function, $\Psi(\boldsymbol{r}, t_f)$, is also projected to scattering states. Finally, the separated wave function and the residual wave function are coherently added up in the momentum space to evaluate the

double differential probability using [76]

$$\mathcal{P}^{(r)}(\boldsymbol{p}) = \frac{d^3W}{dE_p d\Omega_{\boldsymbol{p}}} = \frac{1}{2\pi p}\left|\sum_{l,m}(-i)^l e^{i\delta_l} Y_{lm}(\hat{\boldsymbol{p}}) \int_0^\infty dr \psi_{lm}^{\text{all}}(r,t_f) r R_{pl}(r)\right|^2, \tag{D6}$$

$$\psi_{lm}^{\text{all}}(r,t_f) = \sum_{t_i} U_{\text{Volkov}}(t_f,t_i)\psi_{lm}^{\text{outer}}(r,t_i) + \psi_{lm}(r,t_f), \tag{D7}$$

where $\hat{\boldsymbol{p}} = \boldsymbol{p}/p$ defines the polar and azimuthal angles of the electron momentum, $\delta_l$ stands for the phase shift, and $R_{pl}$ stands for scattering states in the radial coordinate $r$.


[1] P. Agostini, F. Fabre, G. Mainfray, G. Petite, and N. K. Rahman, Free-Free Transitions Following Six-Photon Ionization of Xenon Atoms, Phys. Rev. Lett. **42**, 1127 (1979).

[2] L. F. DiMauro and P. Agostini, Ionization dynamics in strong laser fields, Adv. At., Mol., Opt. Phys. **35**, 79 (1995).

[3] W Becker, F Grasbon, R Kopold, D B Milošević, G G Paulus, and H Walther, Above threshold ionization: From classical features to quantum effects, Adv. At., Mol., Opt. Phys. **48**, 35 (2002).

[4] G. G. Paulus, F. Lindner, H. Walther, A. Baltuška, E. Goulielmakis, M. Lezius, and F. Krausz, Measurement of the Phase of Few-Cycle Laser Pulses, Phys. Rev. Lett. **91**, 253004 (2003).

[5] D. B. Milošević, G. G. Paulus, D Bauer, and W. Becker, Above-threshold ionization by few-cycle pulses, J. Phys. B **39**, R203 (2006).

[6] L. V. Keldysh, Ionization in the field of a strong electromagnetic wave, Zh. Eksp. Teor. Fiz. **47**, 1945 (1964) [J. Exp. Theor. Phys. 92 **20**, 1307 (1965)] .

[7] A. M. Perelomov, V. S. Popov, and M. V.Terent'ev, Ionization of atoms in an alternating electric field, Zh. Eksp. Teor. Fiz. **51**, 309 (1966) [J. Exp. Theor. Phys. **24**, 207 (1967)] .

[8] A. I. Nikishov and V. I. Ritus, Ionization of systems bound by short-range forces by the field of an electromagnetic wave, Zh. Eksp. Teor. Fiz. **50**, 225 (1966) [J. Exp. Theor. Phys. **23**, 168 (1966)] .

[9] D. B. Milošević and F. Ehlotzky, Scattering and reaction processes in powerfull laser fields, Adv. At., Mol., Opt. Phys. **49**, 373 (2003).

[10] A. Becker and F. H. M. Faisal, Intense-field many-body S-matrix theory, J. Phys. B **38**, R1 (2005).

[11] R. Wong, *Asymptotic Approximations of Integrals* (SIAM, Philadelphia, 2001).

[12] L. D. Landau and E. M. Lifshitz, *Quantum Mechanics (Non-relativistic Theory)* (Pergamon Press, Oxford, 1977).

[13] P. Salières, B. Carré, L. Le Déroff, F. Grasbon, G. G. Paulus, H. Walther, R. Kopold, W. Becker, D. B. Milošević, A. Sanpera, and M. Lewenstein, Feynman's path-integral approach for intense-laser-atom interactions, Science **292**, 902 (2001).

[14] V. N. Ostrovsky and D. A. Telnov, Adiabatic theory of multiphoton ionisation. I. Ionisation of an isolated level, J. Phys. B **20**, 2397 (1987).

[15] V. N. Ostrovsky and D. A. Telnov, Adiabatic theory of multiphoton ionisation. II. Resonant phenomena, J. Phys. B **20**, 2421 (1987).

[16] M. Pont, R. Shakeshaft, and R. M. Potvliege, Low-frequency theory of multiphoton ionization, Phys. Rev. A **42**, 6969 (1990).

[17] D. A. Telnov, Adiabatic theory of multiphoton decay in an intense laser field. application to above-threshold photodetachment, J. Phys. B **24**, 2967 (1991).

[18] M. Pont, R. M. Potvliege, R. Shakeshaft, and Z.-j. Teng, Low-frequency theory of multiphoton ionization. ii. general formulation and further results for ionization of H(1s), Phys. Rev. A **45**, 8235 (1992).

[19] O. I. Tolstikhin, T. Morishita, and S. Watanabe, Adiabatic theory of ionization of atoms by intense laser pulses: One-dimensional zero-range-potential model, Phys. Rev. A **81**, 033415 (2010).

[20] O. I. Tolstikhin and T. Morishita, Adiabatic theory of ionization by intense laser pulses: Finite-range potentials, Phys. Rev. A **86**, 043417 (2012).

[21] Y. Okajima, O. I. Tolstikhin, and T. Morishita, Adiabatic theory of high-order harmonic generation: One-dimensional zero-range-potential model, Phys. Rev. A **85**, 063406 (2012).

[22] M. V. Frolov, N. L. Manakov, and A. F. Starace, Analytic formulas for above-threshold ionization or detachment plateau spectra, Phys. Rev. A **79**, 033406 (2009).

[23] M. V. Frolov, D. V. Knyazeva, N. L. Manakov, A. M. Popov, O. V. Tikhonova, E. A. Volkova, M.-H. Xu, L.-Y. Peng, L.-W. Pi, and A. F. Starace, Validity of Factorization of the High-Energy Photoelectron Yield in Above-Threshold Ionization of an Atom by a Short Laser Pulse, Phys. Rev. Lett. **108**, 213002 (2012).

[24] M. V. Frolov, D. V. Knyazeva, N. L. Manakov, J.-W. Geng, L.-Y. Peng, and A. F. Starace, Analytic model for the description of above-threshold ionization by an intense short laser pulse, Phys. Rev. A **89**, 063419 (2014).

[25] A. A. Minina, M. V. Frolov, A. N. Zheltukhin, and N. V. Vvedenskii, Tunnelling approximation for estimating the amplitude of high harmonic generation in intense laser fields: Analysis of ionisation and recombination times, Quantum Electron. **47**, 216 (2017).

[26] M. V. Frolov, N. L. Manakov, E. A. Pronin, and A. F. Starace, Model-Independent Quantum Approach for Intense Laser Detachment of a Weakly Bound Electron, Phys. Rev. Lett. **91**, 053003 (2003).

[27] M. V. Frolov, N. L. Manakov, and A. F. Starace, Effective-range theory for an electron in a short-range potential and a laser field, Phys. Rev. A **78**, 063418 (2008).

[28] N. L. Manakov and L. P. Rapoport, Particle with low binding energy in a circularly polarized field, Zh. Eksp. Teor. Fiz. **69**, 842 (1975) [J. Exp. Theor. Phys. **42**, 430 (1976)] .

[29] N. L. Manakov, V. D. Ovsiannikov, and L. P. Rapoport, Atoms in a laser field, Phys. Rep. **141**, 320 (1986).

[30] N. L. Manakov, M. V. Frolov, A. F. Starace, and I. I. Fabrikant, Interaction of laser radiation with a negative ion in the presence of a strong static electric field, J. Phys. B **33**, R141 (2000).

[31] S.-I. Chu and D. A. Telnov, Beyond the Floquet theorem: Generalized Floquet formalisms and quasienergy methods for atomic and molecular multiphoton processes in intense laser fields, Phys. Rep. **390**, 1 (2004).

[32] R. G. Newton, *Scattering Theory of Waves and Particles*, 2nd ed. (Springer Science & Business Media, New York, 2013).

[33] X. X. Zhou, Z. Chen, T. Morishita, A.-T. Le, and C. D. Lin, Retrieval of electron-atom scattering cross sections from laser-induced electron rescattering of atomic negative ions in intense laser fields, Phys. Rev. A **77**, 053410 (2008).

[34] T. Morishita, A.-T. Le, Z. Chen, and C. D. Lin, Accurate Retrieval of Structural Information from Laser-Induced Photoelectron and High-Order Harmonic Spectra by Few-Cycle Laser Pulses, Phys. Rev. Lett. **100**, 013903 (2008).

[35] D. Ray, B. Ulrich, I. Bocharova, C. Maharjan, P. Ranitovic, B. Gramkow, M. Magrakvelidze, S. De, I. V. Litvinyuk, A.-T. Le, T. Morishita, C. D. Lin, G. G. Paulus, and C. L. Cocke, Large-Angle Electron Diffraction Structure in Laser-Induced Rescattering from Rare Gases, Phys. Rev. Lett. **100**, 143002 (2008).

[36] Z. Chen, A.-T. Le, T. Morishita, and C. D. Lin, Quantitative rescattering theory for laser-induced high-energy plateau photoelectron spectra, Phys. Rev. A **79**, 033409 (2009).

[37] A. Čerkić, E. Hasović, D. B. Milošević, and W. Becker, High-order above-threshold ionization beyond the first-order Born approximation, Phys. Rev. A **79**, 033413 (2009).

[38] C. D. Lin, A.-T. Le, Z. Chen, T. Morishita, and R. Lucchese, Strong-field rescattering physics – self-imaging of a molecule by its own electrons, J. Phys. B **43**, 122001 (2010).

[39] T. Morishita and O. I. Tolstikhin, Adiabatic theory of strong-field photoelectron momentum distributions near a backward rescattering caustic, Phys. Rev. A **96**, 053416 (2017).

[40] D. B. Milošević, A. Čerkić, B. Fetić, E. Hasović, and W. Becker, Low-frequency approximation for high-order above-threshold ionization, Laser Phys. **20**, 573 (2009) .

[41] M. V. Frolov, N. L. Manakov, A. A. Minina, N. V. Vvedenskii, A. A. Silaev, M. Yu. Ivanov, and A. F. Starace, Control of Harmonic Generation by the Time Delay between Two-Color, Bicircular Few-Cycle Mid-IR Laser Pulses, Phys. Rev. Lett. **120**, 263203 (2018).

[42] M. V. Frolov, N. L. Manakov, A. A. Minina, A. A. Silaev, N. V. Vvedenskii, M. Yu. Ivanov, and A. F. Starace, Analytic description of high-order harmonic generation in the adiabatic limit with application to an initial *s* state in an intense bicircular laser pulse, Phys. Rev. A **99**, 053403 (2019).

[43] M. V. Frolov, N. L. Manakov, A. M. Popov, O. V. Tikhonova, E. A. Volkova, A. A. Silaev, N. V. Vvedenskii, and A. F. Starace, Analytic theory of high-order harmonic generation by an intense few-cycle laser pulse, Phys. Rev. A **85**, 033416 (2012).

[44] F. H. M. Faisal, Multiple absorption of laser photons by atoms, J. Phys. B **6**, L89 (1973).

[45] H. R. Reiss, Effect of an intense electromagnetic field on a weakly bound system, Phys. Rev. A **22**, 1786 (1980).

[46] V. S. Popov, Tunnel and multiphoton ionization of atoms and ions in a strong laser field (Keldysh theory), Usp. Fiz. Nauk **174**, 921 (2004) [Phys.-Usp. **47**, 855 (2004)].

[47] L. DiMauro, M. Frolov, K. L. Ishikawa, and M. Ivanov, 50 years of optical tunneling, J. Phys. B. **47**, 200301 (2014).

[48] S. V. Popruzhenko, Keldysh theory of strong field ionization: History, applications, difficulties and perspectives, J. Phys. B **47**, 204001 (2014).

[49] B. M. Karnakov, V. D. Mur, S. V. Popruzhenko, and V. S. Popov, Current progress in developing the nonlinear ionization theory of atoms and ions, Usp. Fiz. Nauk **185**, 3 (2015) [Phys.-Usp. **58**, 3 (2015)] .

[50] G G Paulus, W Becker, W Nicklich, and H Walther, Rescattering effects in above-threshold ionization: A classical model, J. Phys. B **27**, L703 (1994).

[51] W. Becker, A. Lohr, and M. Kleber, Effects of rescattering on above-threshold ionization, J. Phys. B **27**, L325 (1994).

[52] A. Lohr, M. Kleber, R. Kopold, and W. Becker, Above-threshold ionization in the tunneling regime, Phys. Rev. A **55**, R4003 (1997).

[53] S. P. Goreslavskii and S. V. Popruzhenko, Differential photoelectron distributions in a strong elliptically polarized low-frequency laser field, Zh. Eksp. Teor. Fiz. **110**, 1200 (1996) [J. Exp. Theor. Phys. **83**, 661 (1996)].

[54] M. V. Frolov, N. L. Manakov, A. A. Minina, S. V. Popruzhenko, and A. F. Starace, Adiabatic-limit Coulomb factors for photoelectron and high-order-harmonic spectra, Phys. Rev. A **96**, 023406 (2017).

[55] A. A. Radzig and B. M. Smirnov, *Reference Data on Atoms, Molecules, and Ions* (Springer, Berlin, 2012), p. 466.

[56] O. Raz, O. Pedatzur, B. D. Bruner, and N. Dudovich, Spectral caustics in attosecond science, Nat. Photon. **6**, 170 (2012).

[57] D. Faccialà, S. Pabst, B. D. Bruner, A. G. Ciriolo, S. De Silvestri, M. Devetta, M. Negro, H. Soifer, S. Stagira, N. Dudovich, and C. Vozzi, Probe of Multielectron Dynamics in Xenon by Caustics in High-Order Harmonic Generation, Phys. Rev. Lett. **117**, 093902 (2016).

[58] D. Faccialà, S. Pabst, B. D. Bruner, A. G. Ciriolo, M. Devetta, M. Negro, P. P. Geetha, A. Pusala, H. Soifer, N. Dudovich, S. Stagira, and C. Vozzi, High-order harmonic generation spectroscopy by recolliding electron caustics, J. Phys. B **51**, 134002 (2018).

[59] E. Pisanty, M. F. Ciappina, and M. Lewenstein, The imaginary part of the high-harmonic cutoff, J. Phys. Photonics **2**, 034013 (2020).

[60] C. Figueira de Morisson Faria, H. Schomerus, and W. Becker, High-order above-threshold ionization: The uniform approximation and the effect of the binding potential, Phys. Rev. A **66**, 043413 (2002).

[61] S. P. Goreslavskii and S. V. Popruzhenko, Rescattering and quantum interference near the classical cut-offs, J. Phys. B **32**, L531 (1999).

[62] S. P. Goreslavskii and S. V. Popruzhenko, Tunneling limit in the theory of photoelectron rescattering by the parent ion, Zh. Eksp. Teor. Fiz. **90**, 778 (2000).

[63] F. Lindner, M. G. Schätzel, H. Walther, A. Baltuška, E. Goulielmakis, F. Krausz, D. B. Milošević, D. Bauer, W. Becker,

and G. G. Paulus, Attosecond Double-Slit Experiment, Phys. Rev. Lett. **95**, 040401 (2005).

[64] A. Kramo, E. Hasović, D. B. Milošević, and W. Becker, Above-threshold detachment by a two-color bicircular laser field, Las. Phys. Lett. **4**, 279 (2007).

[65] E. Hasović, W. Becker, and D. B. Milošević, Electron rescattering in a bicircular laser field, Opt. Express **24**, 6413 (2016).

[66] D. B. Milošević and W. Becker, Improved strong-field approximation and quantum-orbit theory: Application to ionization by a bicircular laser field, Phys. Rev. A **93**, 063418 (2016).

[67] V.-H. Hoang, V.-H. Le, C. D. Lin, and A.-T. Le, Retrieval of target structure information from laser-induced photoelectrons by few-cycle bicircular laser fields, Phys. Rev. A **95**, 031402(R) (2017).

[68] S. P. Goreslavski, G. G. Paulus, S. V. Popruzhenko, and N. I. Shvetsov-Shilovski, Coulomb Asymmetry in Above-Threshold Ionization, Phys. Rev. Lett. **93**, 233002 (2004).

[69] N. I. Shvetsov-Shilovski, D. Dimitrovski, and L. B. Madsen, Ionization in elliptically polarized pulses: Multielectron polarization effects and asymmetry of photoelectron momentum distributions, Phys. Rev. A **85**, 023428 (2012).

[70] A. M. Perelomov and V. S. Popov, Ionization of atoms in an alternating electrical field. III, Zh. Eksp. Teor. Fiz. **52**, 514 (1967) [J. Exp. Theor. Phys. **25**, 336 (1967)].

[71] V. S. Popov, Imaginary-time method in quantum mechanics and field theory, Phys. At. Nucl. **68**, 686 (2005).

[72] S. V. Popruzhenko, Invariant form of Coulomb corrections in the theory of nonlinear ionization of atoms by intense laser radiation, Zh. Eksp. Teor. Fiz. **145**, 664 (2014) [J. Exp. Theor. Phys. **118**, 580 (2014)].

[73] T. N. Rescigno and C. W. McCurdy, Numerical grid methods for quantum-mechanical scattering problems, Phys. Rev. A **62**, 032706 (2000).

[74] T. J. Park and J. C. Light, Unitary quantum time evolution by iterative Lanczos reduction, J. Chem. Phys. **85**, 5870 (1986).

[75] X. M. Tong, K. Hino, and N. Toshima, Phase-dependent atomic ionization in few-cycle intense laser fields, Phys. Rev. A **74**, 031405(R) (2006).

[76] A. F. Starace, Theory of atomic photoionization, in *Handbuch der Physik*, edited by S. Flugge and W. Mehlhorn (Springer-Verlag, Berlin, 1982), p. 1.